Cell Tissue Res (1984) 235:225–241

Cell and Tissue Research

Ciliated and microvillous structures of rat olfactory and nasal respiratory epithelia

A study using ultra-rapid cryo-fixation followed by freeze-substitution or freeze-etching

Bert Ph. M. Menco
Department of Neurobiology, Northwestern University, Evanston, Illinois, USA*

Summary. The olfactory epithelium of the Sprague-Dawley rat showed structures which indicate that freeze-substitution after ultra-rapid cryo-fixation is a better method for its preservation than conventional fixation techniques. A new feature is that matrices of the distal parts of olfactory cilia range in their staining intensity from very dense to electron-lucent. Outlines of structures are smooth and membrane features can be clearly seen.

The textures of mucus from olfactory and respiratory epithelia are distinctly different after freeze-fracturing and deep-etching following cryo-fixation. Olfactory cilia show no microtubule-attached axonemal structures. Cross-sectional diameters are smaller after freeze-substitution than after freeze-fracturing.

Intramembranous particle densities are lower in nine regions of three cell types in cryo-fixed olfactory and respiratory epithelia than in those chemically fixed and cryo-protected. The fracture faces of membranes from etched, cryo-fixed cells have holes, a result which probably accounts for differences in particle density between cryo-fixed and chemically-fixed, cryo-protected cells. Particle diameters are usually the same using both methods. Densities of intramembranous particles and particles plus holes are highest in supporting cell processes, followed by endings and cilia of olfactory receptor cells, and are lowest in respiratory cilia. Particle densities at outer and inner surfaces are higher than those in either fracture face. Outer surfaces show a good correlation from region to region with densities summated over both fracture faces.

Key words: Cryo-techniques – Olfactory and respiratory epithelia – Cilia – Microvilli – Sprague-Dawley rat

Proteins have been implicated as receptor molecules in olfactory cells (Ma 1981). These molecules may be localized on olfactory cilia (Rhein and Cagan 1981). Phospholipids may also play a major role in olfactory receptor processes (Punter et al. 1981). As yet there is no conclusive evidence for these suggestions; freeze-etch studies may, however, help to resolve this question, as this technique allows the comparison of membrane regions that presumably contain chemosensory receptor sites, with other areas.

In vertebrates, cilia of olfactory receptor cells have been compared with those in non-sensory epithelial cells (Kerjaschki and Hörandner 1976; Menco et al. 1976; Menco 1977, 1980a, b, 1983a; Usukura and Yamada 1978; Breipohl et al. 1982). These authors have found that intramembranous particle densities are higher in olfactory than in respiratory cilia. Similarly, in insects, olfactory cilia have higher densities in regions underneath the pores of exoskeletal hairs than in more proximal regions (Steinbrecht 1980; Menco and Van der Wolk 1982).

All of these studies have dealt with intramembranous features only, whereas chemostimulants probably interact initially with the outer membrane surface (ES; Branton et al. 1975). Since samples used for freeze-fracturing are routinely protected against ice crystal damage, real membrane surfaces have not been observed (Pinto da Silva and Branton 1970; Fisher and Branton 1975). Rapid freezing markedly reduces the formation of ice crystals in the absence of cryo-protection (Plattner and Bachmann 1982; Rash 1983). Following etching, real membrane surfaces, and also cytoplasmic and mucous features, are visualized. Structures can also be studied in a condition approximating the in vivo situation; this has the additional advantage that chemosensory systems need not be exposed to chemostimulatory fixatives.

Rapidly frozen specimens may also be processed by freeze-substitution techniques (Pease 1973; Steinbrecht 1980). Since cryo-fixation and subsequent freeze-substitution of insect olfactory sensilla give superior results to those obtained with conventional techniques (Steinbrecht 1980), it seems desirable to apply this technique to vertebrate olfactory tissue for comparison.

The principal aim of this study has been to compare the freeze-etch appearance of ultra-rapidly frozen olfactory and respiratory epithelium samples (cryo-fixed samples) to that of chemically fixed, cryo-protected samples (protected samples). This comparison has been used in part as a means for the elucidation of artifacts obtained with rapid-freezing techniques. As yet, little attention has been devoted to this matter (Plattner and Bachmann 1982). Three preliminary reports have appeared (Menco 1982a, b, 1983b).

Send offprint requests to: Dr. B. Ph. M. Menco, Department of Neurobiology and Physiology, Northwestern University, Evanston, Illinois 60201, USA

* This work was carried out in the following laboratories: Department of Neurobiology and Physiology, Northwestern University, Evanston, Illinois, USA, Institut für Anatomie, Universitätsklinikum, Essen, FRG, and Psychologisch Laboratorium, Rijksuniversiteit, Utrecht, The Netherlands, and was begun within the Anatomy Section of the 1981 Neurobiology Summer Course at the Marine Biological Laboratories, Woods Hole, Massachusetts, USA

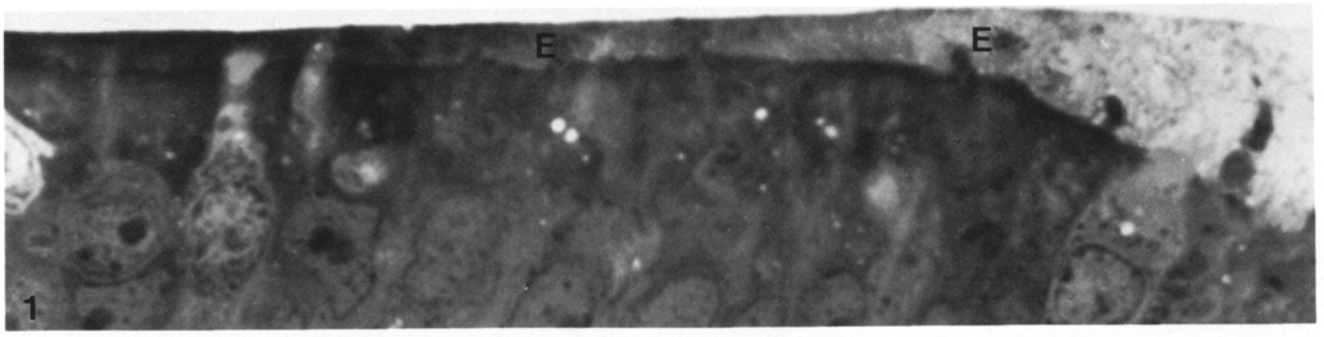
E
E
1

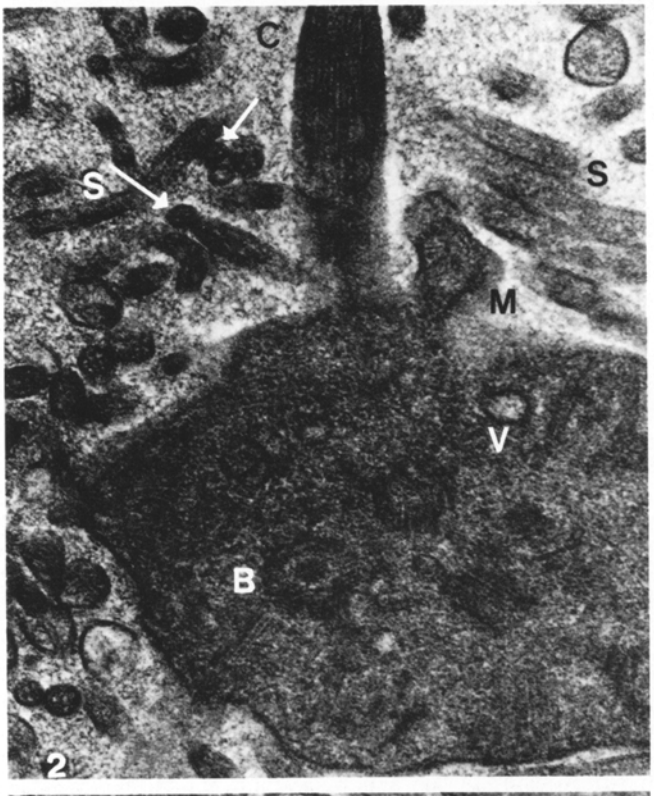
C
S
S
M
V
B
2

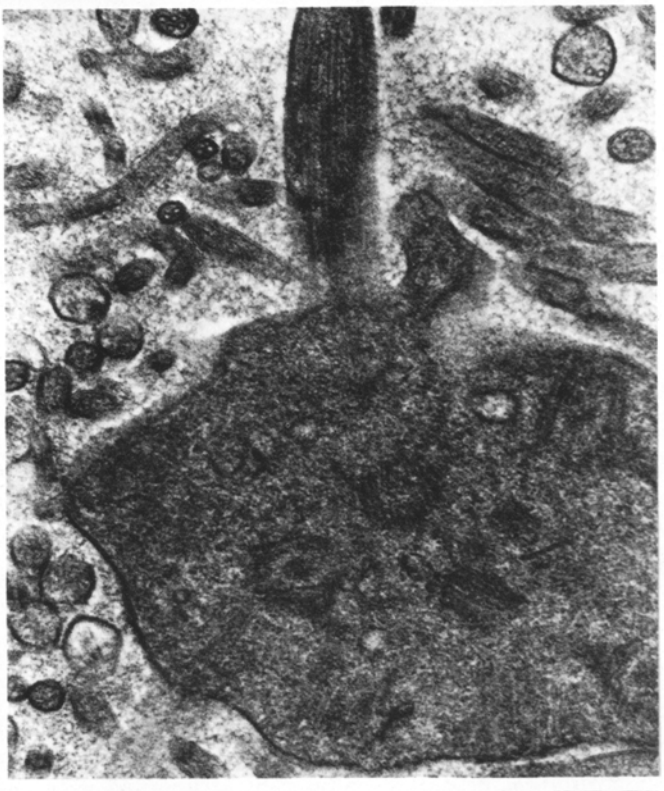

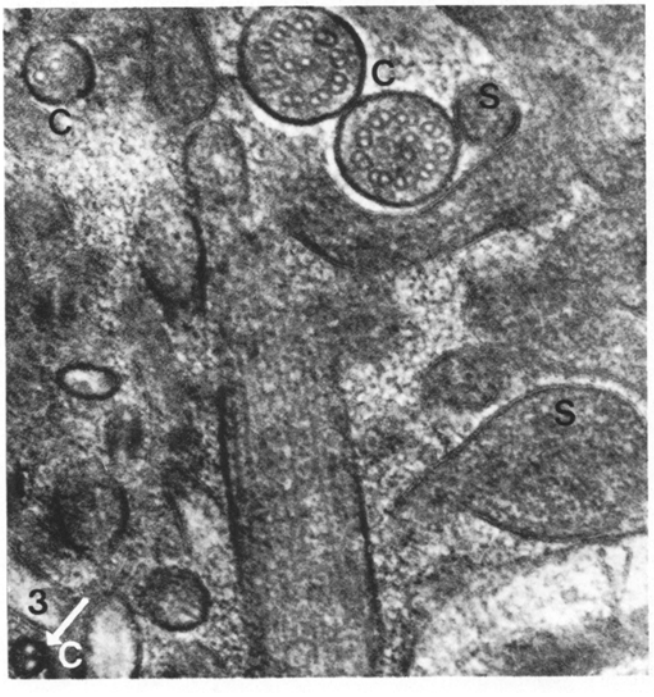
C
C
S
S
3
C

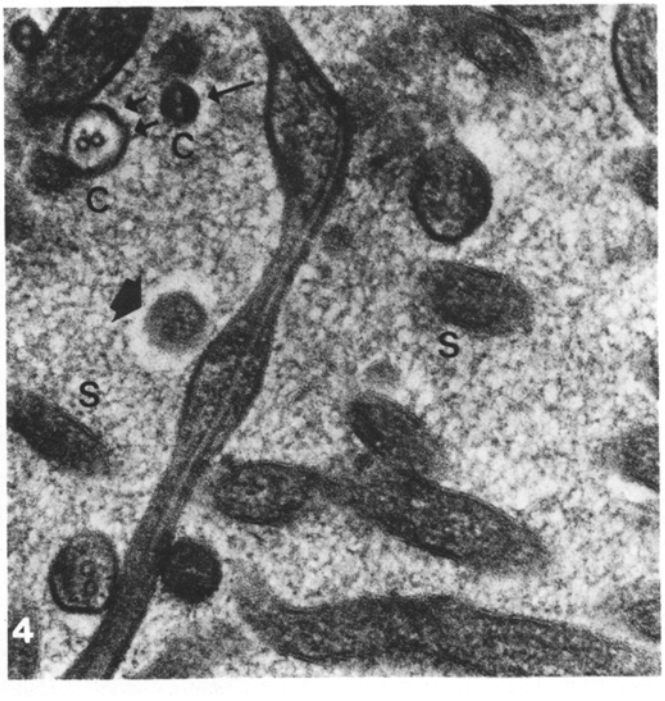
C
C
S
S
4

Table 1. Miscellaneous data related to various structures of cells of olfactory and nasal respiratory epithelium of the rat based on ultra-rapidly frozen, freeze-substituted, and freeze-fractured and deep-etched tissue samples (numbers of animals within brackets)

Structural parameters	Freeze-substitution Olfactory (one)	Freeze-fracturing with deep-etching	
		Olfactory (six)	Respiratory (two)
Diameter, olfactory supporting cells (μm)	– [a]	5.4 ± 2.3^{9} [b]	
Diameter, dendrites (μm)	1.3 ± 0.5^{8}	1.3 ± 0.6^{23}	
Diameter, dendritic endings (μm)	1.3 ± 0.3^{16} * [c]	1.6 ± 0.5^{117}	
Height, dendritic endings (μm)	2.7 ± 1.2^{9}	3.2 ± 0.6^{6}	
Diameter, proximal segments, cilia (μm)	0.21 ± 0.02^{31} *	0.28 ± 0.04^{326}	0.28 ± 0.03^{188}
Length, proximal segments, cilia (μm)	0.9 ± 0.2^{11} *	1.2 ± 0.3^{112} #	6.1 ± 2.7^{6}
Diameter, distal segments, cilia (μm)	0.08 ± 0.02^{48} *	0.11 ± 0.03^{468} #	0.16 ± 0.03^{34}
Length, distal segments, cilia (μm)	–	–	0.50 ± 0.25^{17}
Diameter, olfactory ciliary expansions along shaft (μm)	0.11 ± 0.04^{14} *	0.20 ± 0.09^{207}	
Diameter, olfactory ciliary expansions at tip (μm)	0.11^{1}	0.30 ± 0.14^{73}	
Thickness, olfactory mucus layer (μm)	2.8 ± 1.4^{11}	–	
Vacuole density within dendritic endings (per μm^2)	–	8.6 ± 6.21^{93}	
Diameter, microvilli (μm)	0.09 ± 0.03^{43} * [d]	0.11 ± 0.04^{578} [d]	0.10 ± 0.02^{106} #
Diameter, mucus fibers (nm)	–	14 ± 6^{641}	12 ± 5^{179} #

[a] Could not be determined
[b] Means are presented with their standard deviations; superscripts indicate the number of structures analyzed
[c] For the first two columns significant differences are indicated by *, and for the latter two by #; lowest values bear the sign
[d] Refers to supporting cells

Materials and methods

Twelve male, ten-week-old, Sprague-Dawley rats were used. Tissue from the nasal septum of six of them was subjected to ultra-rapid cryo-fixation only; that of the other six was chemically fixed and cryo-protected before freezing (Menco 1980a; Menco et al. 1980). For ultra-rapid cryo-fixation, tissue samples of about 0.5 cm^2 were placed on holders fitting the freezing head of the fast freezing apparatus and the cooled sample table of the Balzer's freeze-fracture machine. The samples were slam-frozen (Heuser et al. 1979; Heuser 1981) with the epithelium surfaces down. Gelatin (2 mm thick) served as a cushion. Gelatin and tissue were moistened with modified Earles solution (0.1 g $CaCl_2$, 0.2 g KCl, 0.1 g $MgSO_4 \cdot 7H_2O$, 3.4 g NaCl, 0.5 g glucose, 10 mM HEPES/NaOH (Sigma) in distilled H_2O, pH 7.0). The time between killing (decapitation) and cryo-fixation was less than 5 min.

Freeze-fracturing and deep-etching

The samples were put in a Balzer's 360 freeze-fracture apparatus at −150° C, while covered with solidified Freon 22. Freon and frost were removed at −105° C (Müller and Pscheid 1981). At 1.3×10^{-6} mbar and −150° C, the electron guns were degassed with the cooled knife above the sample surface. Fracturing was carried out at −150° C and 1.0×10^{-6} mbar. The tissue was grazed and then the knife was advanced over 10 μm. Etched (5 to 7 min at −105° C) sample surfaces were rotary-replicated at 120 rpm, with platinum/carbon from an electron gun positioned at 45° to the sample, followed by carbon from overhead. Though smaller angles give more detail (Roof and Heuser 1982), 45° was maintained for reasons of comparison (Menco 1980a, b). The samples were immersed in liquid N_2 after removal from the freeze-fracture machine. To minimize sample expansion, a mixture of saturated aqueous NaCl and methanol (about 1:5), solidified in liquid N_2, was prepared. The sample was placed on this mixture. The replica was trimmed and left on its fracture plane through the tissue in the mixture until the tissue became soft. Replicas were cleaned in 40% chromic acid (12 h) and distilled water. They were then transferred by suction using a platinum loop to 400 mesh, hexagonal grids (Gilder, Grantham, U.K.), which were placed on moist filter paper.

Fig. 1. Light micrograph of a section of freeze-substituted, plastic-embedded rat olfactory mucosa, stained with toluidine blue. Compression of the mucus covering the epithelium is obvious when comparing left and right. The surface shows several endings of dendrites of olfactory receptor cells (*E*). Nuclei are those of supporting cells. × 2000

Fig. 2. Stereo-pair of a freeze-substituted dendritic ending of an olfactory receptor cell. The ending contains basal bodies (*B*), sectioned at various levels, electron-lucent vacuoles (*V*), (the indicated one is probably a coated vesicle), proximal parts of two cilia (*C*) and a short microvillus (*M*). Distal parts of the cilia usually have two microtubular fibers and display electron-opaque matrices (*arrows*). Supporting cell microvilli (*S*) surround the sensory ending. × 60000

Fig. 3. Freeze-substituted olfactory cilia (*C*) and supporting cell microvilli (*S*). Except for the microtubules, the cilia do not display much substructure. Their matrices are electron-opaque. Matrices of distal parts of the cilia are even more opaque (*arrow*). One cilium is sectioned longitudinally. Membranes of supporting cell microvilli are less dense than those of the cilia. The mucus has a granular appearance. × 85000

Fig. 4. Freeze-substituted distal parts of olfactory cilia (*C*) and supporting cell microvilli (*S*). The longitudinally sectioned cilium displays lenticular expansions, with microtubules running uninterrupted through them. Cross-sectioned cilia have dense (*one thin arrow*) or electron-lucent (*two thin arrows*) matrices; a microtubular subfiber of the latter cilium displays a small projection. A mucous inclusion surrounded by an electron-lucent halo (*thick arrow*) is present. × 85000

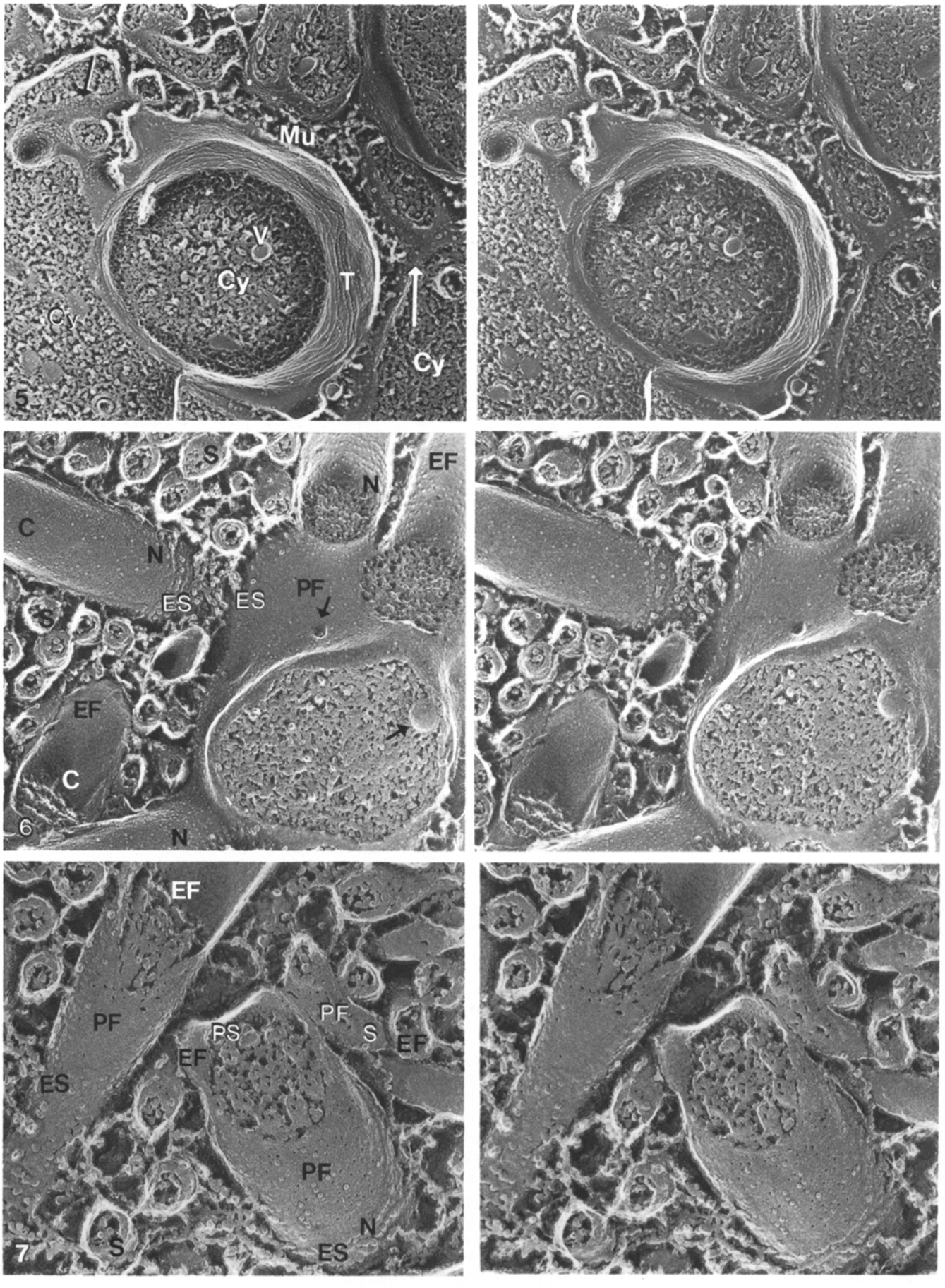
Mu
V
Cy
T
Cy
Cy
5
S
N
EF
C
N
ES
ES
PF
EF
C
6
N
EF
PF
PS
PF
S
EF
EF
ES
PF
N
7
S
ES

Freeze-substitution

Olfactory tissue only was prepared by the freeze-substitution method. Rapidly frozen samples were placed on top of 4% OsO_4 in acetone, solidified in liquid N_2 in a Styrofoam container. The liquid N_2 was allowed to evaporate (as this happens the substitution fluid melts at $-95°$ C). The evaporation took about 6 h, and the samples were left an additional 6 h in the container. They were block-stained with 1% uranylacetate in methanol and subsequently treated according to standard procedures (Pease 1973; Steinbrecht 1980; Ornberg and Reese 1981).

Microscopic observations, photographic procedures and evaluation of results

For light microscopy, thick sections of freeze-substituted samples were stained with toluidine-blue. Ultrathin sections and most of the replicas were examined with a Philips 400 and with JEOL 100C and 200CX electron microscopes, all aquipped with eucentric goniometer stages. Stereo-pairs were prepared by tilting over 6°. Prints were prepared from inverted negatives.

Most quantitative evaluations were carried out at a 170000× final magnification (for methods of calculation see Menco 1980a, b). Numerical comparisons were performed using Student's t test ($P \leqq 0.05$, two sided). For purposes of clarity, main effects rather than detailed individual comparisons have been presented. In Tables 5a, b coefficients of product moment correlation and single factor ANOVA's have been used for a statistical analysis of average densities. The coefficients of product moment correlations have been corrected with the formula

$$r^* = r\left\{1 + \frac{1-r^2}{2(n-2)}\right\} \text{ (Olkin and Pratt 1958),} \quad (1)$$

since the number of values, n, is rather low ($n < 20$). The corrected correlation coefficient is r^*, the original one r.

Results

1. The surface of the olfactory epithelium after cryo-fixation and freeze-substitution

Slam-freezing, as used here for freeze-substitution and freeze-fracturing, gives a considerable compression of the slammed surfaces of the mucus layer covering the surface of the olfactory epithelium (Fig. 1). Ice crystal damage is not conspicuous in that layer. Outlines of structures are smooth, despite the compression (Figs. 2–4). Distal parts of the olfactory cilia show both heavily stained and electron-lucent matrices (Figs. 2–4). Those of the proximal segments are also dense, but less so than those of electron-opaque distal parts (Fig. 3). The typical trilaminar membrane structure can be discerned in supporting cell microvilli, but not in olfactory receptor cell endings and their cilia, where the membranes are rather dense (Figs. 3, 4). The mucus has a fibrous or granular appearance (Figs. 2–4) and has inclusions (Fig. 4). Diameters of cilia and microvilli are significantly smaller than after freeze-fracturing (Table 1).

2. The appearance of olfactory and respiratory epithelial surfaces after cryo-fixation, freeze-fracturing and deep-etching

After etching, the appearance of the cytoplasm within olfactory receptor and supporting cells is that of a compact granular mass (Figs. 5, 6) in which structures such as basal bodies (Fig. 10) can be seen. The mucus has a loose fibrous structure (Figs. 5–10, 12, 13). The mucus covering the respiratory epithelium (Fig. 24) is generally more condensed than that covering the olfactory epithelium. Dimensions of mucus fibers and of other structures of both epithelial types are given in Table 1. For the olfactory epithelium, mucus environments with cilia and microvilli and mucus regions devoid of structures may differ in texture (Fig. 12). Dendritic endings of the olfactory receptor cells have clear tight-junctional belts (Fig. 5) and contain a number of vacuoles (Figs. 2, 5, 6; Table 1); some of these may be coated vesicles (Fig. 2). Whereas respiratory cilia contain microtubule-associated structures in their axonemes (Figs. 25, 26), olfactory cilia have only the microtubules of axonemes in their proximal segments (Figs. 3, 7, 10). The central sheath of respiratory cilia has short projections about 16 nm apart and seems to be twisted. Radial spokes, linked to these projections, repeat at about 30 nm (Fig. 26); arm-like projections are attached to the microtubular doublets (Fig. 25). Tips (Fig. 18) and shafts (Figs. 12, 13, 17, 19) of olfactory cilia have expansions, often giving the shafts the appearance of a beaded string (Fig. 12). In both regions expansions are frequently much wider than the rest of the distal parts of the cilia (Fig. 19). These distal parts of olfactory cilia sometimes branch (Fig. 14). Occasionally the microtubule lattice within the cilia can be seen (Fig. 16).

Ciliary necklaces have been seen in P-faces (Figs. 6, 8, 11, 23), E-faces (Figs. 6, 9) and E-surfaces (Figs. 6, 7). Strand particles stand out less than other ciliary particles in P-faces (Fig. 11). Except for necklaces, E-faces are virtually devoid of particles (Figs. 6, 9). Necklace strands are sometimes present outside the proper necklace region (Fig. 9). Dendritic endings often have necklaces but no other ciliary features (Fig. 9). Ciliary and microvillous E-faces easily collapse (Figs. 13, 22). Apices of the olfactory

Fig. 5. Stereo-pair of a cross-fracture through a dendritic ending of an olfactory receptor cell after freeze-fracturing and deep-etching. Its E-face depicts a tight-junctional belt (*T*). The vacuole (*V*) containing cytoplasm (*Cy*) is denser in appearance than the mucus (*Mu*). The latter is fibrous after etching. P-faces of supporting cell apices have rod-shaped particles (*small arrow*), their E-surfaces display only rounded particles (*large arrow*). The structure indicated with the latter arrow is a microplica of the supporting cell apex. × 40000

Fig. 6. Stereo-pair of a dendritic ending of an olfactory receptor cell, displaying cilia (*C*) and membrane-bounded vacuoles (*arrows*). *P*-faces of cilia have small holes in addition to particles. Their *E*-faces are, except for the necklaces (*N*), virtually devoid of particles. *ES* particles in necklaces and elsewhere are associated with mucus fibers. This is also the case in most of the subsequent micrographs. Supporting cell microvilli (*S*) surround the ending. × 60000

Fig. 7. Stereo-pair of two olfactory cilia, one seen in a proximal region (to the right), the other in a region where the cilium begins to taper. Cilia display *PF, EF, ES* and *PS* features. The P-face of the proximal region has more holes than the tapering one. The former shows an *ES* in the necklace region (*N*) and a *PS* leaflet displaying a high particle density. This cilium shows a complete axoneme, the other one has a reduced number of microtubules. Dynein-arms are absent. The perforated appearance of supporting cell microvilli (*S*) differs from that of the cilia in that the microvilli tend to have larger holes. × 100000

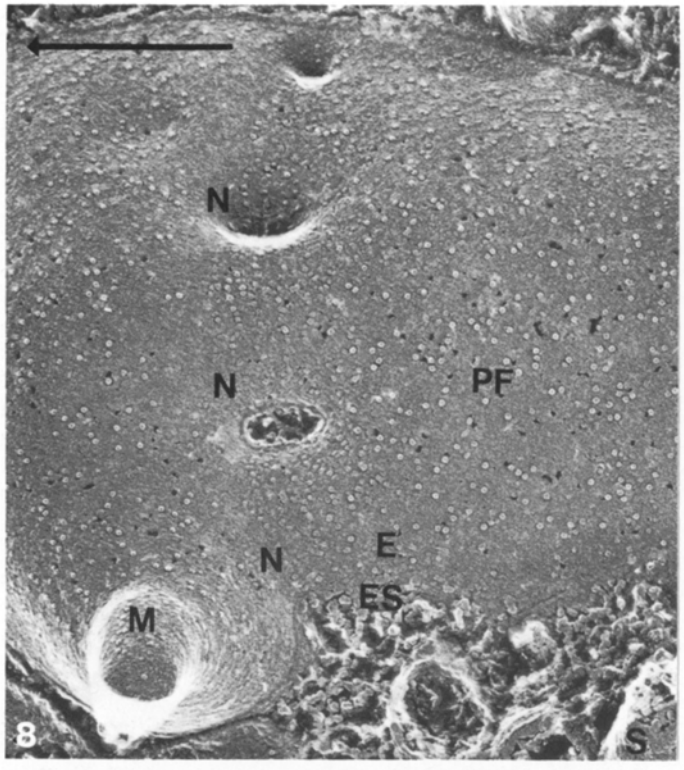
N
N
PF
N
E
ES
M
8
S

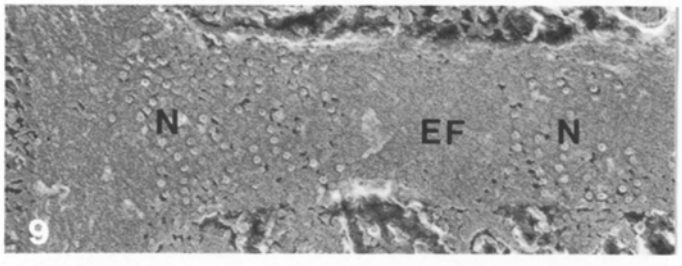
N
EF
N
9

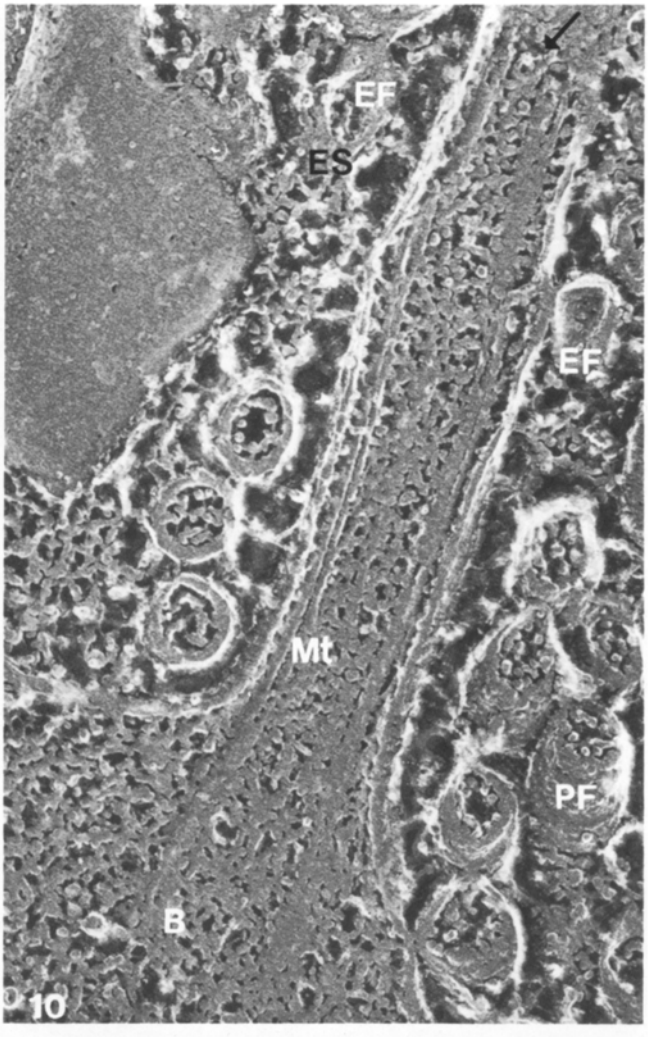
EF
ES
EF
Mt
PF
B
10

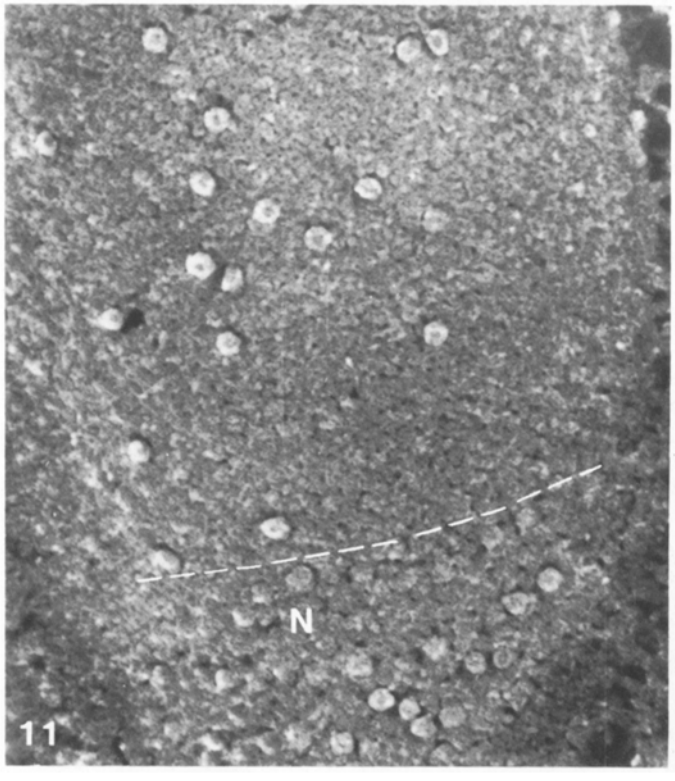
N
11

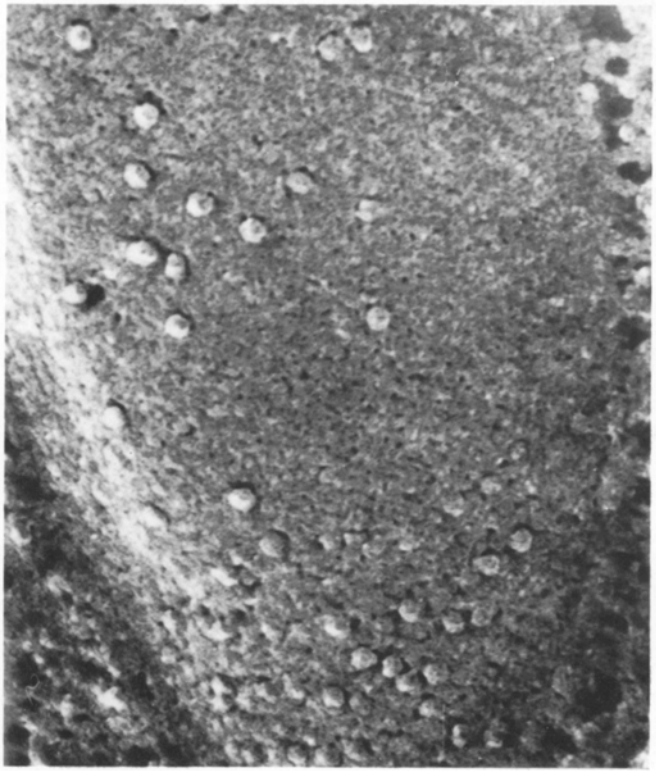

supporting cells have rather deep invaginations, which are virtually devoid of particles. In non-invaginated parts of these apices, P-faces have rod-shaped and globular particles (Fig. 20; Table 2). In addition to microvilli, these apices display microplicae (Fig. 5). Though fewer than in the apices themselves, both structures also have rod-shaped particles in their P-faces. These particles are neither reflected as pits in E-faces nor as particles at external surfaces (Figs. 5, 20; Table 2). Comparison of Figs. 6–10 with Fig. 21 shows that supporting cell microvilli can be quite diverse in shape, a feature also often seen with scanning electron microscopy (unpublished).

In addition to particles, fracture faces in deep-etched samples have small holes in virtually all micrographs. Such holes have not been seen at outer and inner membrane surfaces. The perforated appearance of supporting cell processes differs distinctly from that of receptor cell processes (Figs. 6, 7, 13).

Apart from regions of respiratory cells, intramembranous particle densities are significantly lower in E- than in P-faces. The latter densities are in turn lower than those in E-surfaces (Table 2; Figs. 6, 7, 8, 13, 24, 25), except for those in supporting cell apices. Rod-shaped and globular particles of supporting cell structures have been pooled. PS particle densities are generally higher than fracture face and ES densities; numbers of observations in these surfaces are small, however (Table 2, Figs. 7, 10, and 15).

Particles are distributed similarly over both fracture faces in regions of olfactory receptor endings, whereas holes are not (first four items in Table 3). In respiratory cell processes, particles and holes have a similar distribution; in olfactory supporting cells both entities are distributed differently over apices and microvilli (Table 3). Also, the absolute densities of fracture face particles from the four regions of the olfactory receptor cells are rather similar (Table 2; Figs. 6, 7, 13). This similarity includes poorly developed cilia and short microvilli (Fig. 8). The same is the case for ES particles but not for fracture face holes. EF hole densities are considerably higher than EF particle densities. This contrasts with regions of supporting and respiratory cells where EF particle and hole densities are similar (Table 2). Supporting cell apices have higher PF particle densities than do microvilli. Otherwise both regions show no consistent differences with respect to the distribution of particles and holes. Cilia of respiratory cells have lower P-face particle densities than apices and microvilli (Table 2).

Individual animals show no significant differences in densities of features in fracture faces as the high (0.90–0.99 for the particles and 0.73–0.96 for the holes) and significant ($P \leqq 0.05$) correlation coefficients indicate.

In all planes, except for the PS, particles and holes tend to have highest densities in supporting cell structures (Table 2). This can be seen especially well when densities over both fracture faces are pooled (Table 4). For the fracture faces, supporting cell structures have the highest values and are followed by olfactory receptor cell endings and cilia. Lowest densities are found in the fracture faces of the respiratory cell processes, in particular in the respiratory cilia. ES particle densities of olfactory receptor cell and respiratory cell processes are similar.

Except for the rod-shaped particles of the P-faces of the olfactory supporting cells, ES particles have larger diameters than fracture face particles and holes. ES particles are often associated with mucus fibers (e.g. Figs. 7, 10, 12, 22–24). Both features also have matching diameters, which are smaller in respiratory than in olfactory epithelia (Tables 1, 2). PS particles are usually smaller than those from the ES. For the four regions of the olfactory receptor cells and the two of the supporting cells, diameters of PF particles are significantly larger than those of EF particles, whereas the opposite is true for the holes. Holes in P-faces of proximal parts of olfactory cilia are generally smaller than those in P-faces of distal parts (Fig. 7). Necklace particles have the same diameters in both fracture faces of both types of cilia, but are, like particles in other regions of respiratory cells, smaller than particles in olfactory processes, including those in necklaces of olfactory cilia. Rod-shaped particles of supporting cell apical and microvillous P-faces have the largest diameters (Table 2).

Based on densities and diameters of particles and holes, the three cells differ considerably in appearance of their apical membrane leaflets. Furthermore, supporting cells and respiratory cells have heterogeneous features within the various membrane regions studied (Table 2).

3. A comparison of cryo-fixed and protected samples

The particle densities in fracture faces from protected samples are virtually always significantly higher than those from fracture faces and ES in cryo-fixed samples (Table 2). Fracture-face particles are distributed in similar numbers over both fracture faces with either method, whereas holes, and therefore also particles plus holes, deviate from this distribution (Table 3). Except for those of respiratory structures, diameters of particles in fracture faces are the same with either method. In cryo-fixed samples, ES particles and fracture face particles are smaller in respiratory than in olfactory structures, a distinction not seen in protected samples (Table 2).

The presence of lower particle densities in cryo-fixed

Fig. 8. Ending of an olfactory sensory dendrite with necklace (*N*) features, but no properly developed cilia. The ending has also a short microvillus (*M*) and is surrounded by supporting cell microvilli (*S*). *PF* and *ES* features are visible. Particles are often associated with small ruptures. The *arrow* points towards the base of the ending. × 83000

Fig. 9. *EF* of a proximal part of an olfactory cilium. Apart from necklace features (*N*), present here in two areas, the EF has virtually no particles. × 90000

Fig. 10. Longitudinally fractured olfactory cilium. Except for basal body (*B*) and more distal microtubules (*Mt*), the axoneme is devoid of a clear structure. The PS (*arrow*) has a high particle density. Close to the *arrow*, the circumferences of two microtubules can be seen. Supporting cell microvilli display *PF*, *EF* and *ES* planes. × 70000

Fig. 11. Stereo-pair of a PF of a necklace region (*N*) of an olfactory cilium. Necklace particles (*below the dashed line*) stand out less than other ciliary particles. × 300000

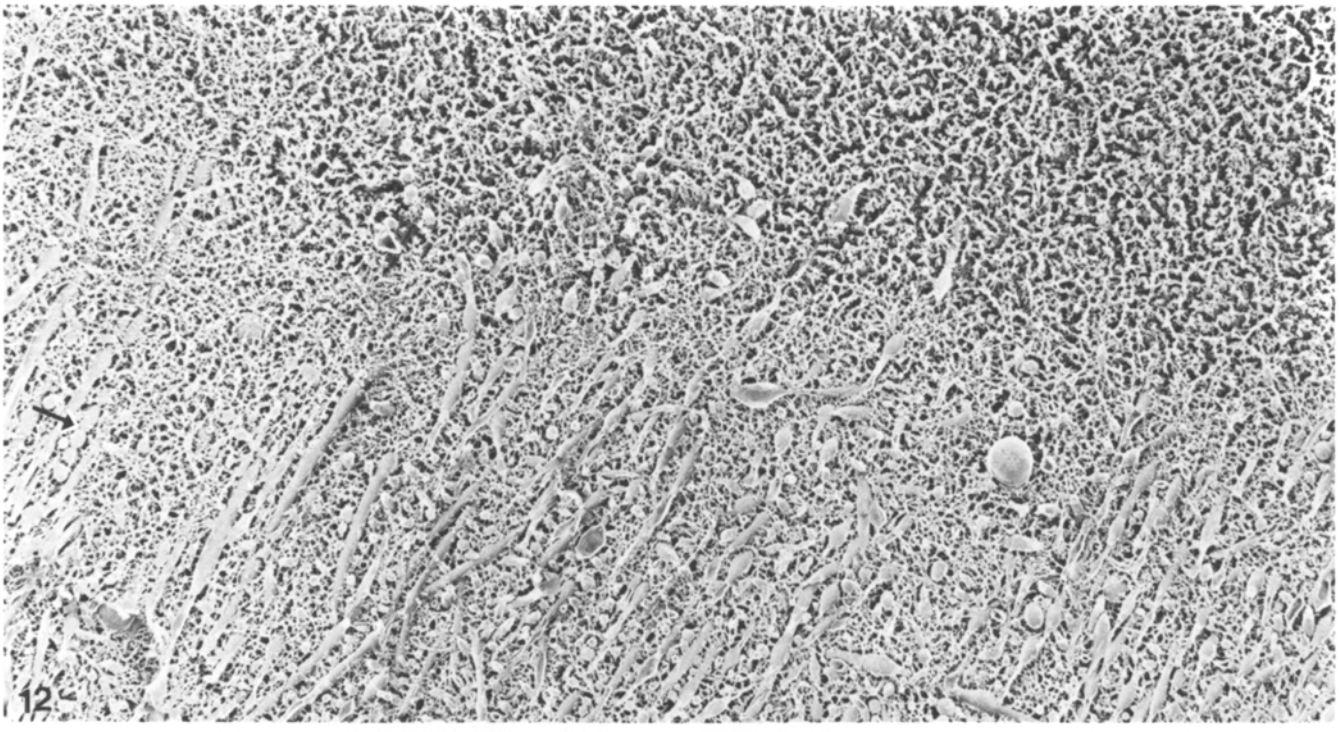

12

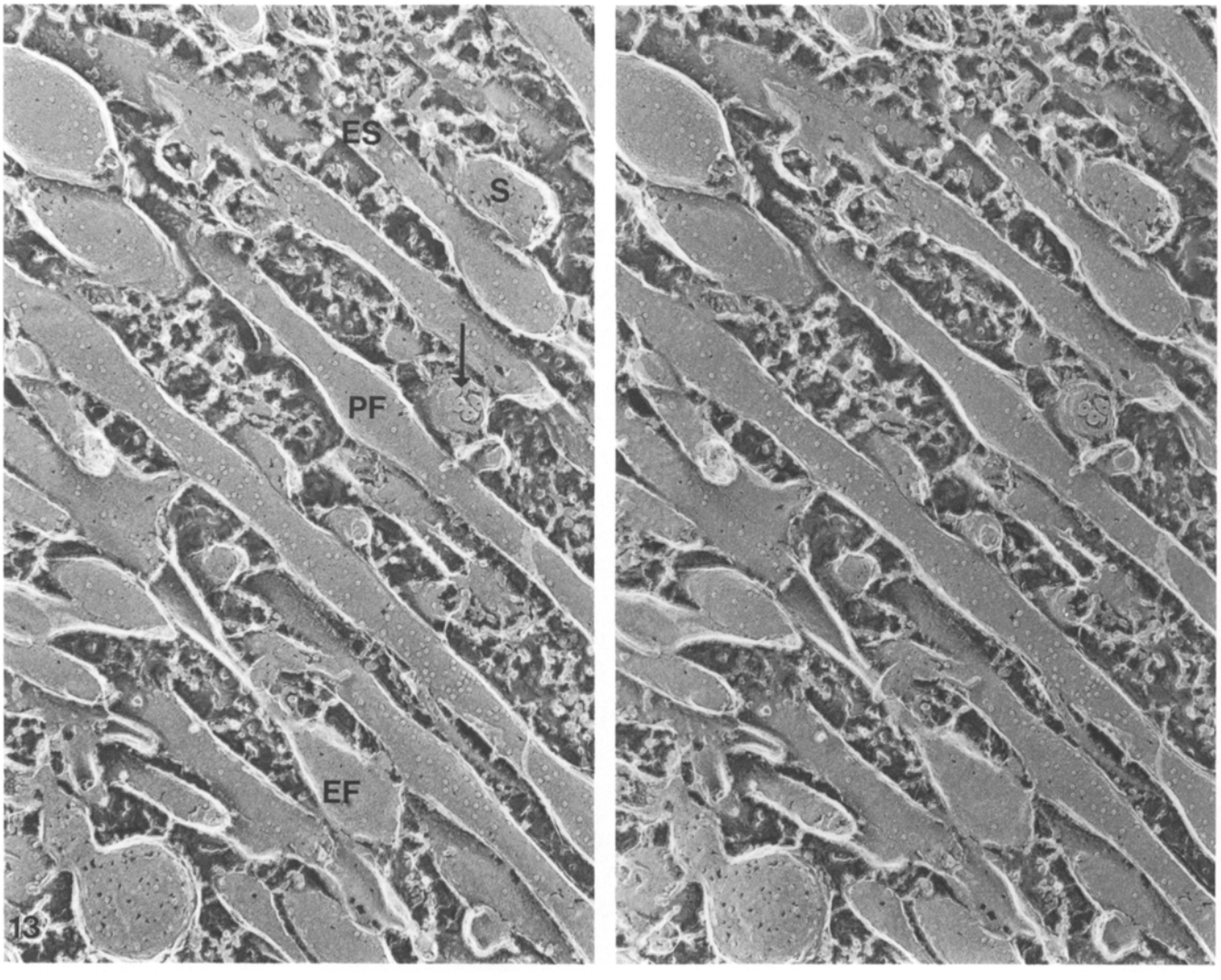

13

Table 2. Densities and diameters of PF, EF, ES and PS particles and holes in cryo-fixed olfactory and nasal respiratory tissue and of PF and EF particles in protected tissue of the Sprague-Dawley rat (numbers of animals within brackets)

	Protected tissue (six)		Cryo-fixed tissue (six olfactory; two respiratory)					
Structures	Intramembranous particles		Intramembranous particles		Intramembranous holes		Membrane surface particles	
	PF	EF	PF	EF	PF	EF	ES	PS
Dendritic ending, olfactory nerve	**0.9±0.4**^{86} [a] *9 ±2*^{86}	**0.3±0.2**^{43} *9 ±2*^{43}	**0.3±0.3**^{180} *10 ±2*^{162}	**0.1±0.2**^{46} *9 ±3*^{36}	**0.4±0.4**^{146} *8 ±4*^{152}	**0.3±0.6**^{43} *9 ±4*^{29}	**0.8±0.5**^{79} *15 ±4*^{95}	–[b] *11 ±4*^{2} [c]
Proximal segment, olfactory cilium	**0.9±0.5**^{87} *9 ±2*^{87}	**0.3±0.2**^{63} *9 ±2*^{63}	**0.3±0.2**^{249} *10 ±2*^{226}	**0.1±0.2**^{112} *9 ±3*^{63}	**0.5±0.5**^{226} *6 ±4*^{225}	**0.3±0.4**^{99} *9 ±7*^{76}	**0.7±0.5**^{136} *14 ±4*^{155}	**1.3±0.4**^{3} *15 ±5*^{6}
Distal segment, olfactory cilium	**0.9±0.4**^{106} 10 ±2^{106}	**0.2±0.2**^{88} *9 ±2*^{88}	**0.4±0.3**^{404} *10 ±2*^{378}	**0.1±0.1**^{241} *9 ±3*^{73}	**0.2±0.2**^{316} *7 ±4*^{271}	**0.5±0.6**^{208} *8 ±5*^{173}	**0.6±0.3**^{261} *15 ±4*^{290}	**2.9±2.9**^{6} *7 ±2*^{6}
Expansion, olfactory cilium	**1.2±0.5**^{28} *10 ±3*^{28}	**0.3±0.3**^{16} *9 ±3*^{12}	**0.5±0.3**^{201} *10 ±2*^{184}	**0.1±0.1**^{43} *9 ±2*^{16}	**0.2±0.3**^{160} *8 ±5*^{144}	**0.7±0.8**^{38} *9 ±4*^{31}	**0.6±0.3**^{70} *15 ±5*^{87}	**1.1±0.6**^{5} *13 ±5*^{6}
Necklace, olfactory cilium	–	–	*10 ±2*^{152}	*11 ±2*^{74}	–	–	*15 ±4*^{94}	–
Apex, olfactory supporting cell	**1.6±0.7**^{42} *18 ±11*^{42}	**0.4±0.3**^{31} *10 ±3*^{31}	**1.2±0.8**^{99} *21 ±3*^{81} [d]	*11 ±2*^{91} [d] **0.3±0.3**^{16} *10 ±2*^{16}	**0.6±0.5**^{78} *13 ±6*^{83}	**0.6±0.5**^{13} *9 ±5*^{13}	**1.0±0.7**^{39} *17 ±6*^{44}	**1.9**[c] *11 ±3*^{2} [c]
Microvillus, olfactory supporting cell	**1.9±0.6**^{96} *13 ±9*^{96}	**0.4±0.2**^{66} *10 ±3*^{66}	**0.5±0.5**^{384} *20 ±4*^{29} [d]	*10±2*^{363} [d] **0.4±0.4**^{254} *9 ±3*^{237}	**0.6±0.4**^{356} *10 ±5*^{359}	**0.4±0.4**^{224} *8 ±4*^{192}	**0.9±0.7**^{271} *15 ±4*^{307}	**0.5±2**^{2} [c] *11 ±1*^{2} [c]
Apex, respiratory columnar cell	**0.8±0.5**^{53} *10 ±4*^{53}	**0.2±0.2**^{26} *9 ±3*^{26}	**0.2±0.2**^{33} *8 ±2*^{35}	**0.1±0.1**^{11} *8 ±3*^{6}	**0.2±0.3**^{28} *10 ±5*^{24}	**0.1±0.1**^{7} *8 ±3*^{2} [c]	**0.3±0.3**^{4} [c] *13 ±2*^{7}	– –
Cilium, respiratory columnar cell	**0.4±0.3**^{141} *9 ±2*^{141}	**0.3±0.3**^{126} *10 ±3*^{126}	**0.1±0.1**^{159} *8 ±2*^{135}	**0.1±0.1**^{123} *8 ±3*^{61}	**0.1±0.3**^{149} *9 ±3*^{116}	**0.1±0.1**^{100} *8 ±3*^{40}	**0.6±0.4**^{100} *11 ±3*^{103}	**1.2±0.4**^{2} [c] *8 ±2*^{2} [c]
Necklace, respiratory cilium	–	–	*9 ±2*^{52}	*8 ±2*^{32}	–	–	*13 ±3*^{7}	–
Microvillus, respiratory columnar cell	**1.6±0.6**^{57} *9 ±2*^{57}	**0.5±0.4**^{59} *10 ±3*^{59}	**0.3±0.3**^{87} *8 ±2*^{79}	**0.2±0.3**^{57} *8 ±2*^{38}	**0.2±0.3**^{74} *9 ±4*^{61}	**0.1±0.3**^{44} *7 ±3*^{21}	**0.7±0.4**^{45} *11 ±3*^{51}	– –

[a] First line indicates densities of intramembranous particles per $\mu m^2 \times 10^{-3}$; second line *italics* indicates particle diameters in nanometers
[b] –: No observations
[c] Based on few observations (less than five)
[d] Diameters of supporting cell apex and microvillus PF particles in unfixed material have been split into those which are ≧than 15 nm and those which are <15 nm in order to emphasize a bimodal distribution of these diameters (Menco 1980b)

samples than in protected samples was accompanied by the presence of holes with the former method. Therefore, it was thought that holes represent, at least in part, lost particles. In many instances small ruptures were found next to particles (e.g. Figs. 7, 8, 13, 20). In order to analyse this, particle and hole densities summated over both fracture faces of the nine regions of the three cell types of the Sprague-Dawley rat considered in this study, are presented separately and combined. In addition the ES and PS particle densities in those regions and the pooled particle density values over both fracture faces in protected samples are provided (Table 4). This table also gives PF+EF particle density values in several other animals (Menco 1980b, 1983a). Fracture face particle densities, particle plus hole densities and external surface particle densities in cryo-fixed samples correlate significantly with particle densities in protected samples. However, for the absolute values only those of particle plus holes in cryo-fixed tissue do not significantly differ from those of particles in protected tissue (Table 5a). Comparison of the first and sixth columns of Table 4 with summated particle densities over both fracture faces of the same nine regions in protected samples in a different strain of rat (Wistar) and three other vertebrate species (Columns 7–10 in Table 4) shows that virtually all correlation coefficients are significant, and except for that of the dog, the absolute distributions do not differ significantly (Table 5b). Therefore, particle and hole densities in deep-etched material are probably inversely related, implying that holes can,

Fig. 12. The mucus layer of the olfactory epithelium after deep-etching. Regions with cilia (bottom half) are more compact than areas devoid of cilia (top half). Mucus fibers are granular. Distal parts of the cilia often have a beaded appearance (*small arrow*). ×12500

Fig. 13. Stereo-pair of tapering elements of olfactory cilia displaying *PF, EF* and *ES* features. The cilia have lenticular expansions; different cilia have differing *PF* particle densities. P-faces here have fewer holes than those in more proximal regions (Fig. 7). The *PF* appearance of microvilli (*S*) differs markedly from that of the cilia. A cross-fractured cilium (*arrow*) shows three microtubules. ×67000

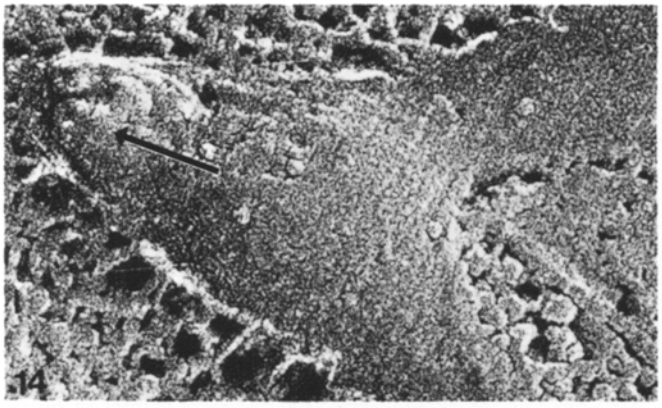

14

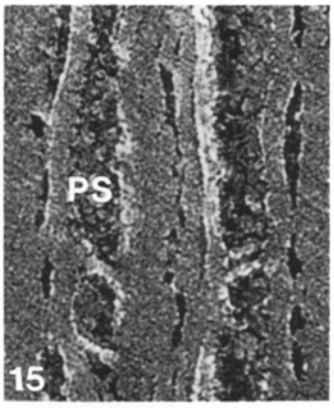

15

16

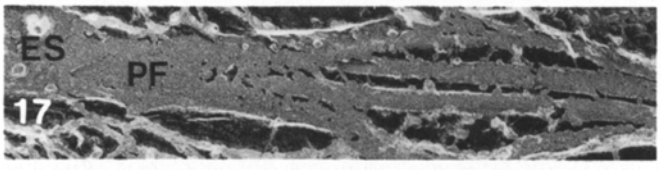

17

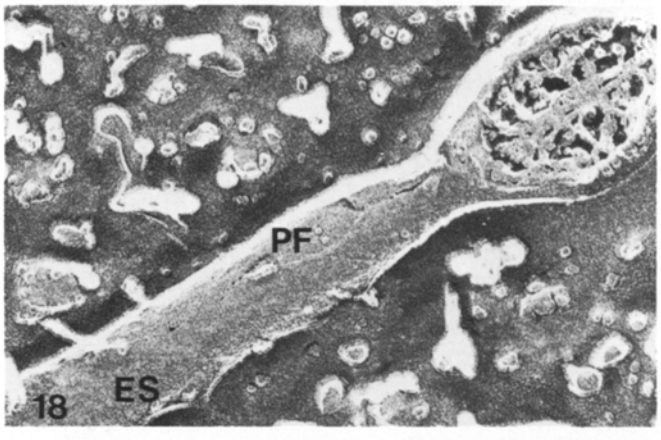

18

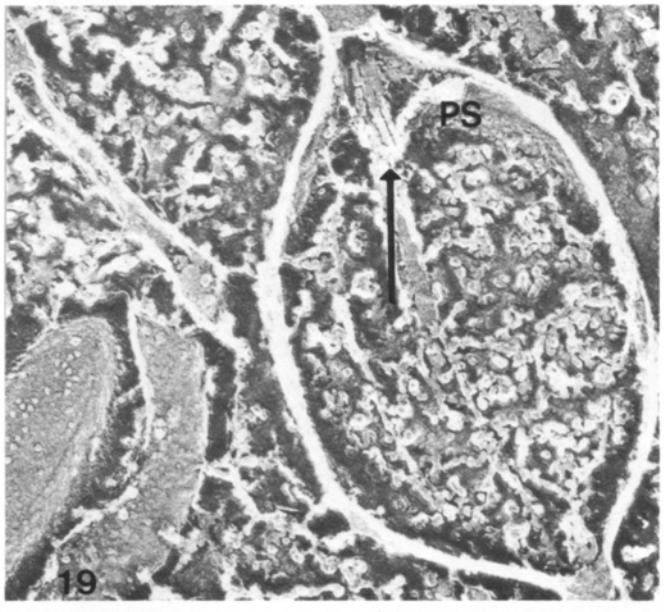

19

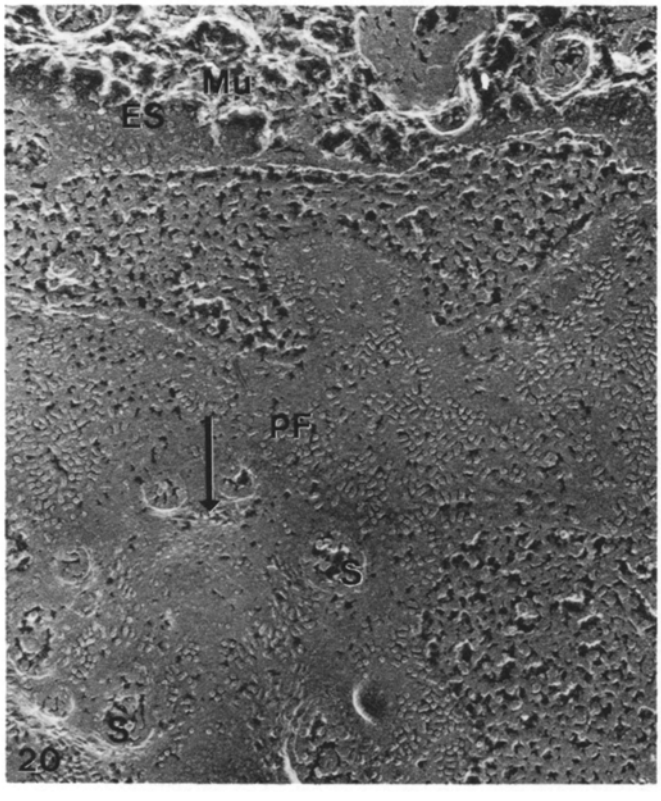

20

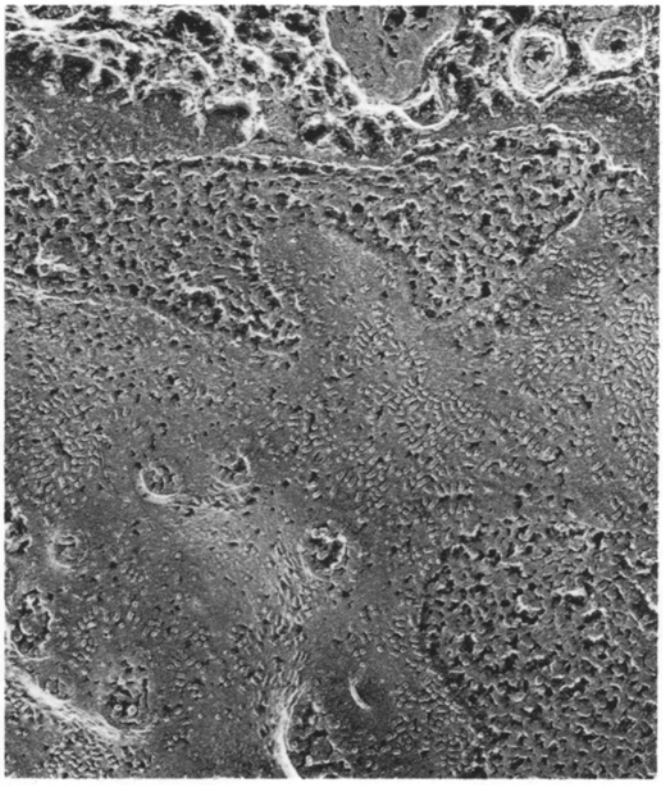

Table 3. Fractions of P-face particle, hole, and particle plus hole densities as a percentage of P + E-face densities for various regions of three cells of the olfactory and nasal respiratory epithelial surfaces of cryo-fixed tissue samples and protected tissue samples (numbers of animals within brackets)

Structures	Protected tissue (six)	Cryo-fixed tissue (six olfactory; two respiratory)		
	Particles	Particles	Holes	Particles + holes
Dendritic ending, olfactory nerve	75	75	57	64
Proximal segment, olfactory cilium	75	75	63	67
Distal segment, olfactory cilium	82	80	29	50
Expansion, olfactory cilium	80	83	22	47
Apex, olfactory supporting cell	80	80	50	67
Microvillus, olfactory supporting cell	83	56	60	58
Apex, respiratory columnar cell	80	67	67	67
Cilium, respiratory columnar cell	57	50	50	50
Microvillus, respiratory columnar cell	76	60	67	63

at least in part, be counted as lost particles. If this is done, densities in cryo-fixed and protected material resemble each other (Tables 4, 5).

Discussion

1. The olfactory epithelium surface after freeze-substitution

The slamming action needed for cryo-fixing the tissue (Heuser et al. 1979; Heuser 1981) compresses the mucus layer of the olfactory epithelium to half its original thickness (Fig. 1; Table 1; Menco 1980a). Although the appearance of structures within this layer seems not to be seriously affected, as Figs. 2 and 3 suggest, distortion of the mutual relationship between structures and deformation of structures cannot be excluded (Pinto da Silva and Kachar 1980).

Diameters of structures are smaller after freeze-substitution than after freeze-fracturing (Table 1); this implies that shrinking occurs even though structure outlines are smooth (Figs. 3, 4). Such shrinking is found with all techniques requiring dehydration (Menco 1977, 1983a; Lidow and Menco 1984). An effect of the rapid rate of substitution on dimensions of structures cannot be excluded. Dimensions of structures in freeze-fractured, fixed, cryo-protected samples resemble those in cryo-fixed, freeze-fractured samples (Table 1; Menco 1980a, 1983a), implying that the freezing procedure does not affect dimensions. As in insects (the moth *Bombyx mori*, Steinbrecht 1980), circumferences of olfactory of rat are smooth after freeze-substitution. In contrast to the expanded distal elements of *Bombyx* olfactory cilia, which are electron-lucent (Steinbrecht 1980), the thin distal elements of rat olfactory cilia often have electron-opaque matrices (Figs. 2–4), a feature so far seen only with freeze-substitution. It seems that the distal segments contain substances that are easily lost with conventional fixation and dehydration procedures (e.g. Kerjaschki 1976; Menco 1977; Moran et al. 1982).

The dense appearance of membranes of olfactory cilia when compared with those of microvilli of olfactory supporting cells (Figs. 3, 4) is shared with membranes of equivalent structures in insects subjected to freeze-substitution (Steinbrecht 1980). The observations corroborate freeze-etch results, in that membranes of both structures have a different distribution of particles and holes (Tables 2–5; Figs. 6, 7, 10, 13).

Apart from the mucus compression, the structures present in the olfactory epithelium are better preserved with freeze-substitution than with conventional fixation techniques. This is in agreement with Steinbrecht's (1980) conclusion on insect olfactory structures.

2. Particles at outer and inner membrane surfaces, and mucous and cytoplasmic features

Relative distributions of ES, and PF plus EF particles (and also of particles and holes) over several regions of various

Fig. 14. Branching olfactory cilium. This distal segment shows a PF and contains two microtubules (*arrow*). × 150000

Fig. 15. *PS* of tapering element of olfactory cilium with a high particle density. × 200000

Fig. 16. Microtubules within a distal element of an olfactory cilium displaying a subunit lattice pattern. The EF underneath the microtubules has many holes. × 250000

Fig. 17. Narrow expansion along the shaft of an olfactory cilium. The expansion contains microtubules (compare with Fig. 4). *PF* and *ES* features are visible. × 95000

Fig. 18. Club-shaped tip of olfactory cilium containing microtubules. *PF* and *ES* features are visible. × 90000

Fig. 19. Wide expansion along the shaft of an olfactory cilium with other cilia in its vicinity. Part of the longitudinally running microtubules has been fractured away (*arrow*). The *PS* demonstrates a high particle density. × 75000

Fig. 20. Stereo-pair of the apex of an olfactory supporting cell. Microvilli (*S*) have been fractured away. The *PF* has patches of mostly rod-shaped particles, which appear pinched at the middle. Small ruptures are often present near particles. Dimples (*arrow*) are virtually devoid of particles. The *ES* shows globular particles and no holes. The mucus (*Mu*) has a loose fibrous appearance. × 60000

Table 4. A comparison of particle and hole densities from cryo-fixed olfactory and nasal respiratory tissue of the Sprague-Dawley rat with densities from protected tissue of the same rat strain, of the Wistar rat, the beagle dog, ox and frog[a] (numbers of animals within brackets)

Structures	Summated density values per $\mu m^2 \times 10^{-3}$									
	Cryo-fixed, Sprague-Dawley rat (six)[b]					Protected, particle densities, PF + EF				
	Particle densities			Hole densities	Particle + hole densities	Sprague-Dawley rat (six)	Wistar rat (six)[b]	Beagle dog (seven)	Ox (three)	Frog (four)
	PF + EF	ES	PS	PF + EF	PF + EF					
Dendritic ending, olfactory nerve	0.4^{226}[c]	0.8^{79}	–[d]	0.7^{189}	1.1^{415}	1.2^{129}	1.6^{61}	2.4^{50}	–	0.9^{34}
Proximal segment, olfactory cilium	0.4^{361}	0.7^{136}	1.3^{3}	0.8^{325}	1.2^{686}	1.2^{150}	1.6^{105}	2.4^{83}	1.4^{55}	1.0^{150}
Distal segment, olfactory cilium	0.5^{645}	0.6^{261}	2.9^{6}	0.7^{524}	1.2^{1169}	1.1^{194}	1.6^{225}	2.4^{109}	1.6^{93}	1.0^{146}
Expansion, olfactory cilium	0.6^{244}	0.6^{70}	1.1^{5}	0.9^{198}	1.5^{442}	1.5^{44}	1.8^{71}	2.6^{25}	1.7^{32}	1.2^{15}
Apex, olfactory supporting cell	1.5^{115}	1.0^{39}	1.9^{1}	1.2^{91}	2.7^{206}	2.0^{73}	2.4^{48}	3.0^{25}	1.7^{13}	2.3^{27}
Microvillus, olfactory supporting cell	0.9^{638}	0.9^{271}	0.5^{2}	1.0^{580}	1.9^{1218}	2.3^{162}	3.0^{171}	3.9^{175}	2.7^{55}	3.3^{123}
Apex, respiratory columnar cell	0.3^{44}	0.3^{4}	–	0.3^{35}	0.6^{79}	1.0^{79}	1.3^{37}	1.6^{40}	0.8^{12}	1.2^{6}
Cilium, respiratory columnar cell	0.2^{282}	0.6^{100}	1.2^{2}	0.2^{249}	0.4^{531}	0.7^{267}	1.0^{144}	1.3^{181}	1.0^{67}	0.4^{6}
Microvillus, respiratory columnar cell	0.5^{144}	0.7^{45}	–	0.3^{118}	0.8^{262}	2.1^{116}	2.5^{105}	2.4^{147}	1.2^{57}	2.2^{29}

[a] See Menco 1980b, 1983a; Menco et al. 1980
[b] Respiratory samples of the cryo-fixed Sprague-Dawley rat are based on two animals and those of the Wistar rat on ten animals
[c] Standard deviations are not presented. Superscripts indicate total numbers of observations
[d] –: Observations lacking

cells correlate significantly (Table 5a). This indicates that membrane outer surface particles represent molecular entities that are related to fracture face particles. However, the count of the ES particles may not be accurate because of the contribution of condensed mucus to the particle population, a feature which would give rise to an overcount. ES particles and mucus fibers have similar diameters: both are larger in olfactory than in respiratory epithelia (Tables 1, 2). The deep-etch morphology of respiratory cilia (Figs. 22, 24, 25) resembles that of *Tetrahymena* somatic cilia. Both have E-surfaces with a bumpy appearance and fracture faces that are smooth (Goodenough and Heuser

Fig. 21. Olfactory supporting cell microvilli. These look quite different from those in, e.g., Figs. 6–10. The mucus has a fibrillar appearance and spreads loosely in a fan-like manner from the microvillous E-surfaces. × 27000

Fig. 22. Respiratory cilia (*C*) and microvilli (*R*). Membranes of both structures display *PF* and *ES* features. The microvilli also show *EF* features. Mucus fibers (*Mu*) are associated with *ES* particles. × 50000

Fig. 23. The *PF* of the apex of a respiratory cell and of some cilia showing necklaces (*N*) and a few particles above necklace regions. × 85000

Fig. 24. Stereo-pair of distal regions of respiratory cilia showing *PF*, *EF* and *ES* features. *PF* and *EF* are virtually devoid of particles; the *ES* has a bumpy appearance. The *PF* shows few holes. The cilia end in blunt, conical tips (bottom). The mucus (*Mu*) has a compact appearance. × 70000

Fig. 25. Stereo-pair of cross-fractured respiratory cilia and microvilli (*R*). Ciliary axonemes display the typical 9(2) + 2 microtubule subfiber structure; dynein-arms are attached clockwise to the A-subfibers of the doublets (*arrowheads*). Ciliary P- and E-faces are smooth; the *ES* has a granular appearance. × 113000

Fig. 26. Longitudinally fractured respiratory cilium. Doublet subfibers and small projections of the central sheath (*thick arrow*) are bridged by radial spokes. The central sheath seems to be twisted (*dashed line*). Particles attached to the doublet subfibers are possibly dynein-arms (*small arrow*). × 140000

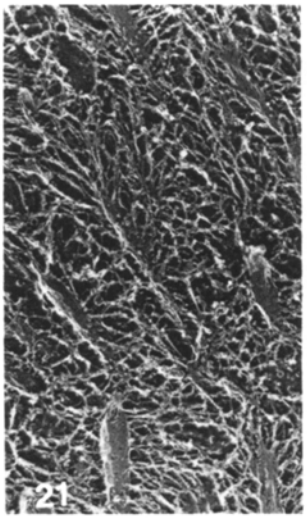
21

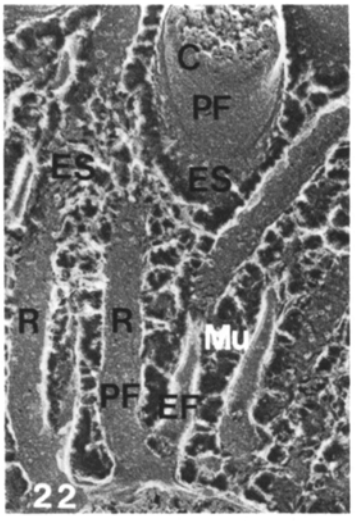
C
PF
ES
ES
R
R
Mu
PF
EF
22

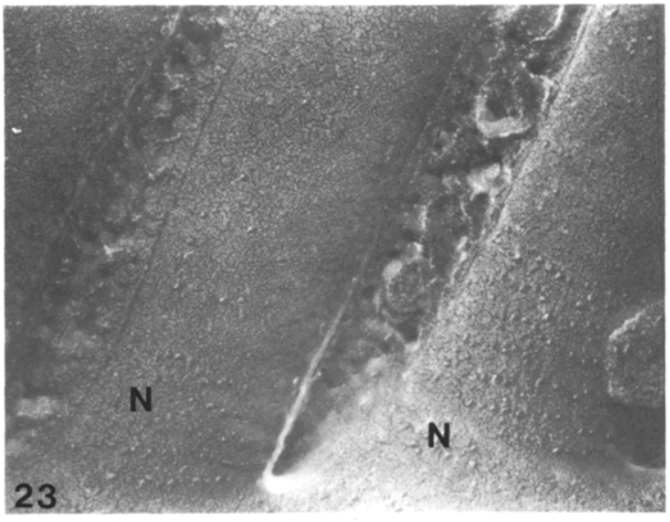
N
N
23

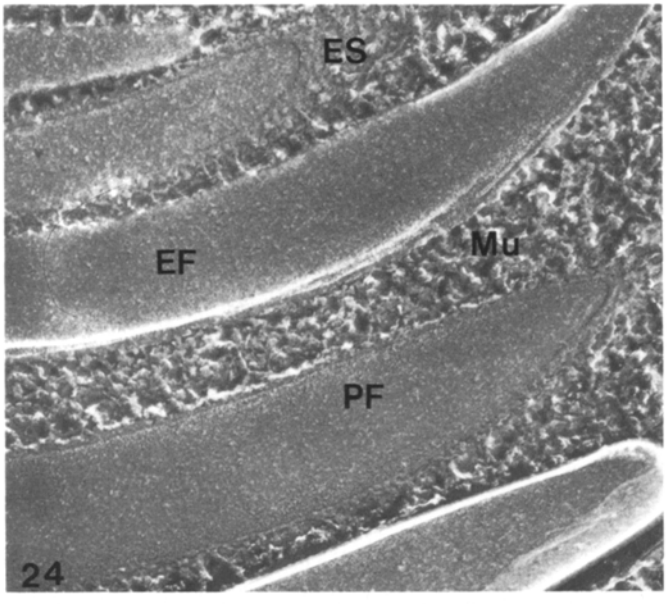
ES
EF
Mu
PF
24

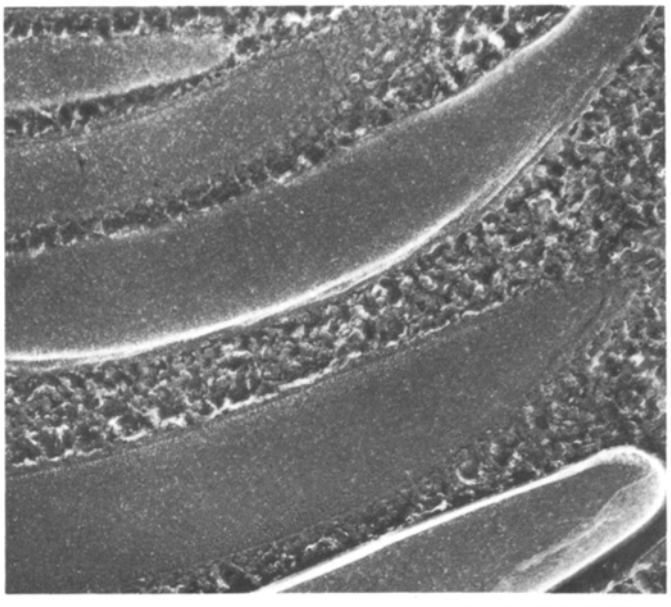

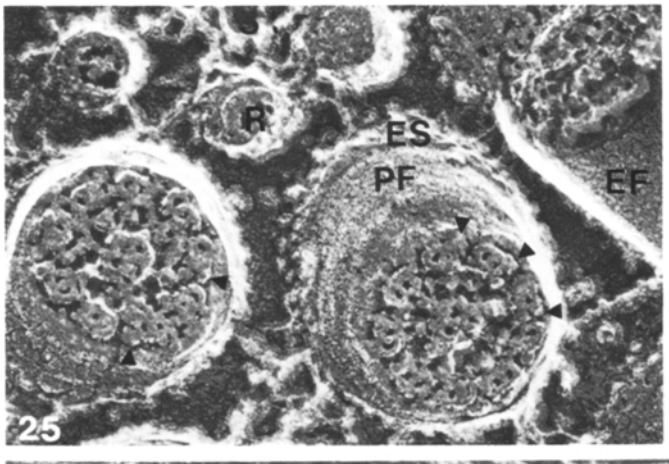
R
ES
PF
EF
25

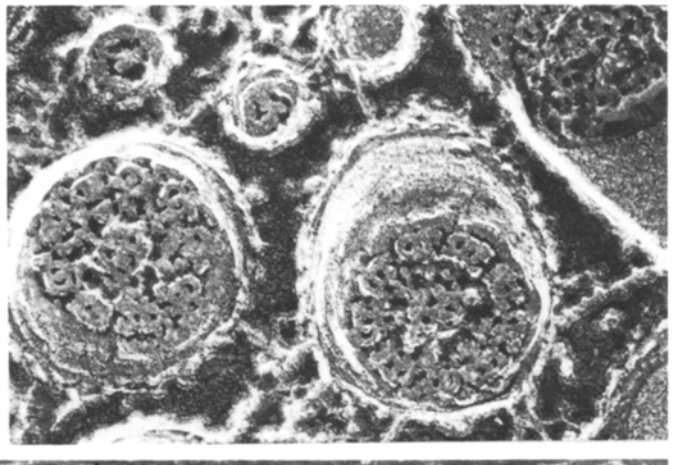

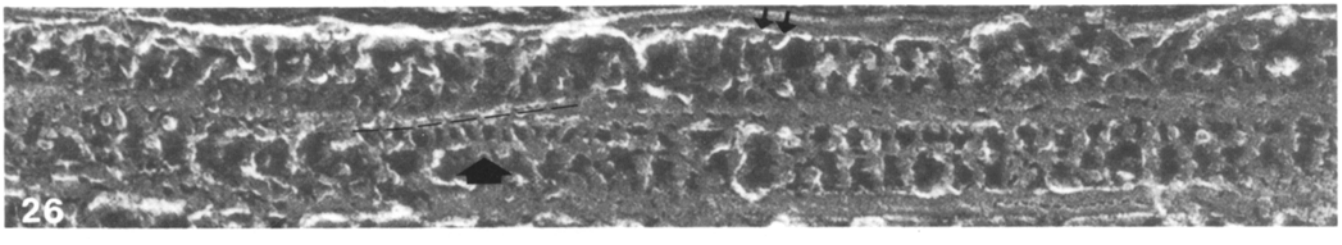
26

Table 5. Correlations (r^*) and their significance levels and significance levels of the variance ratios (F-values) based on single factor ANOVA's of the matrix of Table 4 regarding particle and hole densities in membranes of olfactory and respiratory epithelial structures of the Sprague-Dawley rat in cryo-fixed and protected samples (**a**) and in cryo-fixed and protected samples of that strain and various other animals (**b**)

Table 5a

	Statistic	Cryo-fixed tissue				
		Particle densities			Hole densities	Particle + hole densities
		PF + EF	ES	PS	PF + EF	PF + EF
Protected tissue, particle densities PF + EF	Coefficient of product moment correlation, r^* [a]	0.71	0.69	0.37	0.55	0.69
	Significance of r^*	0.05	0.05	–[b]	–	0.05
	Significance of F	0.001	0.001	0.001	0.001	–

Table 5b

Particle densities in protected samples PF + EF	Statistic	Cryo-fixed, particle + hole densities PF + EF	Protected, particle densities PF + EF	Protected, particle densities PF + EF		
		Sprague-Dawley rat		Wistar rat	Beagle dog	Ox
Sprague-Dawley rat	Coefficient of product moment correlation, r^* [a]	0.69				
	Significance of r^*	0.05				
	Significance of F	–[b]				
Wistar rat	Coefficient of product moment correlation, r^*	0.69	0.99			
	Significance of r^*	0.05	0.001			
	Significance of F	–	–			
Beagle dog	Coefficient of product moment correlation, r^*	0.83	0.91	0.99		
	Significance of r^*	0.01	0.01	0.001		
	Significance of F	0.001	0.01	–		
Ox	Coefficient of product moment correlation, r^*	0.72	0.71	0.76	0.94	
	Significance of r^*	0.05	0.05	0.05	0.001	
	Significance of F	–	–	–	0.01	
Frog	Coefficient of product moment correlation, r^*	0.66	0.95	0.97	0.87	0.75
	Significance of r^*	–	0.001	0.001	0.01	0.05
	Significance of F	–	–	–	0.01	–

[a] Since the r-values are based on a small number of values (≤ 9 per column in Table 4), they have been corrected (See Formula 1 in Materials and methods)

[b] Not significant at levels ≤ 0.05

1982). This further strengthens the argument that surface protuberances cannot be due to mucus condensation. It is also possible that the mucus gives rise to an undercount by masking particles.

In *Torpedo* post-synaptic membranes, surface protuberances also match fracture face particles (Heuser and Salpeter 1979), though in photoreceptor disk membranes, luminal surface particle densities are considerably higher than those in P-faces, wich suggests fracture face particle aggregation (Roof and Heuser 1982).

The appearance of mucus of olfactory epithelium differs from that of respiratory epithelium (Figs. 5, 10, 12, 13, 24), implying that each has a different composition (Cuschieri and Bannister 1974). A variety of solutes appears fibrous after etching (Miller et al. 1983). Since Earle's solution has been used here for rinsing the samples, the contribution of this solute has to be taken into account as far as the appearance of the mucus network is concerned.

PS particles tend to occur in high densities in nearly all structures observed and correlate neither with fracture face particles and holes nor with ES particles (Tables 4, 5). The high densities are in agreement with other studies where P-surfaces have been examined (e.g. Gulley and Reese 1981). In those studies, such particles are shown to be closely associated with several types of cytoskeletal elements. Associations similar to those between mucus fibers and ES particles apply also to cytoplasmic elements and PS particles.

3. Particles and holes in membrane fracture faces

In the cell types studied here, the sums of particles and holes over both fracture faces in the cryo-fixed samples correlate well with the summated particle densities over both fracture faces in protected samples (Table 5). This is strong evidence that the holes mostly correspond to lost particles. Moreover, small ruptures are often found next to particles (Figs. 5, 8, 20), implying that particles are often in the process of being removed.

It is known that holes are a true etching artifact (Verkleij and Ververgaert 1975). In the absence of etching, holes are not observed (Heuser et al. 1979; Heuser and Reese 1981). These studies also suggest that holes are not caused by the slamming action. Moreover, slam-frozen, chemically fixed and cryo-protected sea urchin eggs have no holes in fracture faces (Chandler and Heuser 1979), whereas, in the absence of cryo-protection and with deep-etching, holes are present in chemically fixed samples (Chandler and Heuser 1981). Pinto da Silva (1973) has demonstrated that, as a consequence of etching, depressions occur in regions of particles. Engstrom, as cited by Pinto da Silva et al. (1973), hypothesizes that "a wind of subliming water molecules traverses pits left during membrane splitting by the removal of intercalated particles preferentially associated with the opposite fracture face."

Removal of particles, resulting in the formation of holes may involve the following factors. Changes in dimensions of membrane lipids and proteins as a consequence of differing coefficients of expansion can lead to rupture at interfaces between them. Hydrophilic cores of integral proteins can contain water, causing dimensional changes during freezing. Pinto da Silva (1973) states that particles provide a preferential pathway for passage of water molecules. Water molecules can push the particles out of the membrane leaflet during sublimation. Finally, the fracturing process can cause a loss of particle forming elements (Easter et al. 1983), and during etching holes can be formed in regions where particles are removed. Hole sizes are thus a function of the type of membrane and rates of freezing and etching (Fujikawa 1981).

In the processes of olfactory receptor cells, E-faces are more susceptible to hole formation than P-faces (Tables 2, 3), which are probably better protected by cytoskeletal elements underneath (Satir and Satir 1979). Longer etching periods presumably lead to a different distribution of holes and particles over the fracture faces.

In contrast to the present findings, studies on erythrocytes have demonstrated lower intramembranous particle densities in protected cells than in unprotected cryo-fixed but not ultra-rapidly frozen cells. Unlike the results of the present study, the differences are not dramatic and occur mainly in E-faces (Furcht and Scott 1975; Parish 1975; Plattner and Bachmann 1982). Holes can also occur in regions of pits opposite membrane-intercalated particles (Pinto da Silva et al. 1973). Pits are seen opposite the rod-shaped particles in apices of olfactory supporting cells in protected material (Menco 1980b). Since such pits are not encountered here, they are probably ruptured during etching, resulting in holes according to the hypothesis of Pinto da Silva et al. (1973). Variations like these account for the lack of precise correlations in Table 5.

Apart from those in respiratory structures, diameters of intramembranous particles in cryo-fixed and protected samples are similar (Table 2; Menco 1980b, c) and, since particle diameters in rotary-shadowed and unilaterally shadowed material are virtually the same (Simpson 1979), particle diameters seem generally not to be affected by chemical fixation and glycerination procedures.

4. Other membrane features

A distinction has been made between expansions of olfactory cilia with particles and those with smooth fracture faces (Menco 1980a, b). The smooth type has rarely been encountered during the present study, suggesting that this type may often be an artifact (Hay and Hasty 1979). Branching of cilia (Fig. 14) has not been demontrated previously in vertebrate olfactory cilia but is common in those of insects (Steinbrecht 1980; Menco and Van der Wolk 1982). In insects, these branches show the same beaded appearance (Steinbrecht 1980) as distal elements of vertebrate olfactory cilia (Figs. 4, 12, 13).

In protected samples (Menco 1980b, 1983a), but not in cryo-fixed material (Figs. 24, 25; Table 2), respiratory cilia often have more particles in E- than in P-faces. This may be due to an aggregation of subunits into particles in E-faces during chemical fixation. Respiratory cilia may have a whole array of membrane proteins. This is suggested by biochemical analysis of ciliary membranes of *Paramecium* spp., where about 70 proteins are found (Adoutte et al. 1980). The freeze-fracture appearance of these cilia, however, resembles that of respiratory cilia in that only few particles are present (Allen 1978). Therefore, many membrane proteins may be too small for detection with freeze-fracture methods. Pretreatment makes some of them more prominent because of aggregation.

Necklaces of cilia in olfactory and respiratory epithelia have the same appearance (except for particle diameters (Table 2)) in protected and cryo-fixed samples, i.e. seven and five strands respectively. Since necklace particles are often present in E-faces (Fig. 9; Table 2) and since in P-faces they protrude less from the ciliary membrane leaflet than any other particles (Fig. 11), they probably represent truly transmembranous particles (Menco 1980c). Most metazoan cilia, whether sensory or not, have several necklace strands (Menco 1980c), whereas protozoan cilia usually have only two strands (Bardele 1981). Strands scattered above regular necklace regions, as seen here in olfactory cilia (Fig. 9), occur also in non-sensory cilia (Boisvieux-Ulrich et al. 1977; Breipohl et al. 1980). Necklace formation without the presence of properly developed cilia (Fig. 8; Menco 1980a, c) appears to be a frequent event, as scanning electron microscope investigations demonstrate (unpublished).

Although the typical basket shape of coated vesicles (Heuser and Evans 1980) inside receptor cell endings and in apical regions of supported cells could not be clearly demonstrated (Figs. 5, 6), observations on thin sections in perfused material show that both structures do depict such vesicles (unpublished).

Supporting cell apices have microplicae in addition to microvilli in insects (Menco and Van der Wolk 1982) and in vertebrates (Fig. 5). The shape and distribution of the rod-shaped particles in the P-faces of these apices is not affected by the method of sample preparation (Fig. 20; Kerjaschki and Hörandner 1976; Menco 1980b); this has also been found for similar particles in toad urinary bladder

cells (Wade 1976). They are truly P-face-bound and have never been found in any of the other planes. Particles similar in shape occur in cell membranes of apices and microvilli of supporting cells of the vomeronasal chemosensory organ (Breipohl et al. 1982). It has been suggested that they play a role in hormone-related processes (Wade 1976; Menco 1980a).

5. Axonemal features of olfactory and respiratory epithelia

Rat respiratory cilia have about the same distance between projections in their axonemal central sheath as cilia of *Tetrahymena* (16 nm). The repeat period of radial spokes is also similar (30 nm) but a triplet grouping of these spokes as found in *Tetrahymena* could not be discerned (Fig. 26; Warner 1981). The central sheath in Fig. 26 appears to be twisted. This is probably not an artifact, since twisting of central microtubules has been demonstrated in cilia and flagella of unicellular organisms (Omoto and Kung 1981). Microtubules of the distal elements of olfactory cilia (Fig. 16) have a similar lattice pattern to negatively stained (Warner 1981) and deep-etched (Goodenough and Heuser 1982) microtubules of protozoan cilia and flagella. The lattice repeat is about 4 nm (Warner 1981). According to Goodenough and Heuser (1982) mammalian nasal respiratory cilia display, like protozoan cilia and flagella, a five component substructure of their outer dynein-arms. Although the density of the cytoplasmic matrix may obscure axonemal substructures other than the 9(2)+2 pattern in olfactory cilia, the absence of dynein-arms (Figs. 3, 7) can be verified using other techniques (Menco 1983a; Lidow and Menco 1984). Motility needing such arms is therefore not essential for proper olfactory functioning, even though olfactory cilia in species in other vertebrate orders have dynein-arms and can be motile (Breipohl et al. 1980; Mair et al. 1982; Menco 1983a; Lidow and Menco 1984).

6. Concluding remarks

The similarities in density and diameters between intramembranous particles in samples prepared by ultra-rapid cryo-fixation and those prepared by freezing techniques needing protection suggest that the freeze-fracture method does not drastically affect the particle distributions, at least if one counts the intramembranous holes as particles. For endings and cilia of olfactory sensory cells this would mean that concentrations of putative olfactory receptors in cryo-fixed samples, match those estimated previously from protected samples (Menco 1980b). Since ES particle densities are similar to those in fracture faces (Tables 4, 5), this would also be true for these particles. Such estimates may be used as a guide for biochemical studies (Menco 1980b).

However, it is unlikely that biochemical events following stimulation with odorous compounds are simply reflected at an ultrastructural level, since a preliminary study, in which samples of olfactory epithelium were exposed to odorous stimuli just before cryo-fixation, did not provide any indication that such events can be directly visualized at the level of the receptor endings and their cilia. Receptor labeling may resolve this problem.

Acknowledgements. The author is grateful to Drs. W. Breipohl (Essen), A.I. Farbman and F. Gonzales (Evanston), E.P. Köster and A.J. Verkleij (Utrecht) for research facilities and discussions. Barbara Mlynek (Essen) and the OMI (Utrecht) are acknowledged for photographic assistance and Wim van As and Ellen Lovell for computer and typing assistance, respectively.

Funding has been provided by the Section of Functional Neuroanatomy, N.I.N.C.D.S., N.I.H., by Program Project 1-PO1-NS-18490 from the N.I.H., U.S. Public Health Service, by Grant Br. 358/5-1 of the Deutsche Forschungsgemeinschaft and by the Dutch Social Security System.

References

Adoutte A, Ramanathan R, Lewis RM, Dute RR, Ling K-Y, Kung C, Nelson DL (1980) Biochemical studies of the excitable membrane of *Paramecium tetraurelia*. III. Proteins of cilia and ciliary membranes. J Cell Biol 84:717–738

Allen RD (1978) Membranes of ciliates: Ultrastructure, biochemistry and fusion. In: Poste G, Nicolson GL (eds) Cell surface reviews, Vol 5, Membrane fusion. North-Holland Publ Co, Amsterdam NY Oxford, pp 657–763

Bardele CF (1981) Functional and phylogenetic aspects of the ciliary membrane: A comparative freeze-fracture study. Biosystems 14:403–421

Boisvieux-Ulrich E, Sandoz D, Chailly B (1977) A freeze-fracture and thin section study of the ciliary necklace in quail oviduct. Biol Cellulaire 30:245–252

Branton D, Bullivant S, Gilula NB, Karnovsky MJ, Moor H, Mühlethaler K, Northcote DH, Packer L, Satir B, Satir P, Speth V, Staehlin LA, Steere RL, Weinstein RS (1975) Freeze-etching nomenclature. Science 190:54–56

Breipohl W, Mendoza AS, Miragall F (1980) Freeze-etching studies on the ciliary necklace in the rat and chick. J Anat 130:801–807

Breipohl W, Mendoza AS, Miragall F (1982) Freeze-fracturing studies on the main and vomeronasal olfactory sensory epithelia in NMRI-mice. In: Breipohl W (ed) Olfaction and endocrine regulation, IRL Press Ltd, London, pp 309–322

Chandler DE, Heuser JE (1979) Membrane fusion during secretion. Cortical granule exocytosis in sea urchin eggs as studied by quick-freezing and freeze-fracture. J Cell Biol 83:91–108

Chandler DE, Heuser JE (1981) Postfertilization growth of microvilli in the sea urchin egg: New views from eggs that have been quick-frozen, freeze-fractured, and deeply etched. Dev Biol 82:393–400

Cuschieri A, Bannister LH (1974) Some histochemical observations on the mucosubstances of the nasal glands of the mouse. Histochem J 6:543–558

Easter DW, Wade JB, Boyer JL (1983) Structural integrity of hepatocyte tight junctions. J Cell Biol 96:745–749

Fisher K, Branton D (1975) Application of the freeze-fracture technique to natural membranes. Methods Enzymol 32:35–44

Fujikawa S (1981) Cooling rates on the membrane of frozen human erythrocytes. In: Morris GJ, Clarke A (eds) Effects of low temperatures on biological membranes. Academic Press, NY London, pp 323–344

Furcht LT, Scott RE (1975) Modulation of the distribution of plasma membrane intramembranous particles in contact-inhibited and transformed cells. Biochim Biophys Acta 401:213–220

Goodenough UW, Heuser JE (1982) Substructure of the outer dynein arm. J Cell Biol 95:798–815

Gulley RL, Reese TS (1981) Cytoskeletal organization at the postsynaptic complex. J Cell Biol 91:298–302

Hay ED, Hasty DL (1979) Extrusion of particle-free membrane blisters during glutaraldehyde fixation. In: Rash JE, Hudson CS (eds) Freeze fracture: Methods, artifacts and interpretations. Raven Press, NY, pp 59–66

Heuser JE (1981) Preparing biological samples for stereo-microscopy by the quick-freeze, deep-etch, rotary-replication technique. In: Turner JN (ed) Methods in cell biology. Vol 22. Three-dimensional ultrastructure in biology. Academic Press, NY London, pp 97–122

Heuser JE, Evans L (1980) Three dimensional visualization of coated vesicle formation in fibroblasts. J Cell Biol 84:560–583

Heuser JE, Reese TS (1981) Structural changes after transmitter release at the frog neuromuscular junction. J Cell Biol 88:564–580

Heuser JE, Salpeter SR (1979) Organization of acetylcholine recep-

tors in quick-frozen, deep-etched and rotary-replicated *Torpedo* post-synaptic membrane. J Cell Biol 82:150–173
Heuser JE, Reese TS, Dennis MJ, Jan Y, Jan L, Evans L (1979) Synaptic vesicle exocytosis captured by quick freezing and correlated with quantal transmitter release. J Cell Biol 81:275–300
Kerjaschki D (1976) The central tubuli in distal segments of olfactory cilia lack dynein arms. Experientia 32:1459–1460
Kerjaschki D, Hörandner H (1976) The development of mouse olfactory vesicles and their cell contacts: A freeze-etching study. J Ultrastruct Res 54:420–444
Lidow MS, Menco BPhM (1984) Observations on olfactory and respiratory cilia in frogs and rats using tannic acid-supplemented fixation and photographic rotation. J. Ultrastruct. Res. In Press.
Ma WC (1981) Receptor membrane function in olfaction and gustation: Implications from modification by reagents and drugs. In: Norris DM (ed) Perception of behavioral chemicals. Elsevier Biomedical Press, Amsterdam, pp 267–287
Mair RG, Gesteland RC, Blank DL (1982) Changes in olfactory receptor cilia morphology and physiology during development. Neuroscience 7:3091–3103
Menco BPhM (1977) A qualitative and quantitative investigation of olfactory and nasal respiratory mucosal surfaces of cow and sheep based on various ultrastructural and biochemical methods. Communications Agricultural University Wageningen, The Netherlands 77–13:1–157
Menco BPhM (1980a) Qualitative and quantitative freeze-fracture studies on olfactory and nasal respiratory structures of frog, ox, rat and dog. I. A general survey. Cell Tissue Res 207:183–209
Menco BPhM (1980b) Qualitative and quantitative freeze-fracture studies on olfactory and nasal respiratory epithelial surfaces of frog, ox, rat and dog. II. Cell apices, cilia and microvilli. Cell Tissue Res 211:5–30
Menco BPhM (1980c) Qualitative and quantitative freeze-fracture studies on olfactory and respiratory epithelial surfaces of frog, ox, rat and dog. IV. Ciliogenesis and ciliary necklaces (including high-voltage observations). Cell Tissue Res 212:1–16
Menco BPhM (1982a) The ultrastructure of rat olfactory and nasal respiratory epithelium surfaces after ultra-rapid cryo-fixation. In: Electron microscopy 1982, Vol 3, Biology. Deutsche Gesellschaft für Elektronenmikroskopie e.V., Frankfurt/Main, pp 187–188
Menco BPhM (1982b) Ultra-rapid freezing, freeze-fracturing, deep-etching and rotary-shadowing on rat olfactory and respiratory epithelium surfaces. Proc 5th ECRO Congress, Regensburg, p 48
Menco BPhM (1983a) The ultrastructure of olfactory and nasal respiratory epithelium surfaces. In: Reznik G, Stinson SF (eds) Nasal tumors in animals and man. Vol 1. Anatomy, physiology and epidemiology. CRC Press Inc, Boca Raton FL, pp 45–102
Menco BPhM (1983b) Ultra-rapid freezing studies on rat olfactory and nasal respiratory epithelia. Proc 5th AChems Meeting, Sarasota FL, Abstract 94
Menco BPhM, Van der Wolk FM (1982) Freeze-fracture characteristics of insect gustatory and olfactory sensilla. I. A comparison with vertebrate olfactory receptor cells with special reference to ciliary components. Cell Tissue Res 223:1–27
Menco BPhM, Dodd GH, Davey M, Bannister LH (1976) Presence of membrane particles in freeze-etched bovine olfactory cilia. Nature 263:597–599
Menco BPhM, Laing DG, Panhuber H (1980) Strain- or sample-dependent variations in intramembranous particle densities using freeze-fracturing on aldehyde-fixed, cryoprotected olfactory and nasal respiratory epithelium surface structures. In: Van der Starre H (ed) Olfaction and taste VII. Information Retrieval Ltd, London Washington DC, p 93
Miller KR, Prescott CS, Jacobs TL, Lassignal NL (1983) Artifacts associated with quick-freezing and freeze-drying. J Ultrastruct Res 82:123–133
Moran DT, Rowley JC III, Jafek BW, Lovell MA (1982) The fine structure of the olfactory mucosa in man. J Neurocytol 11:721–746
Müller W, Pscheid P (1981) An improved freeze-fracturing procedure preventing contamination artifacts at fracturing temperatures below 163 K (−110° C) in an unmodified Balzers unit. Mikroskopie (Wien) 39:143–148
Olkin I, Pratt JW (1958) Unbiased estimation of certain correlation coefficients. Ann Math Statist 29:201–211
Omoto CK, Kung C (1980) Rotation and twist of the central-pair microtubules in the cilia of *Paramecium*. J Cell Biol 87:33–46
Ornberg RL, Reese TS (1981) Beginning of exocytosis captured by rapid freezing of *Limulus* amebocytes. J Cell Biol 90:40–54
Parish GR (1975) Changes of particle frequency in freeze-etched erythrocyte membrane after fixation. J Microsc (Oxf) 104:245–256
Pease DC (1973) Substitution techniques. In: Koehler JK (ed) Advanced techniques in biological electron microscopy. Springer, Berlin Heidelberg NY, pp 35–66
Pinto da Silva P (1973) Membrane intercalated particles in human erythrocyte ghosts: Sites of preferred passage of water molecules at low temperature. Proc Natl Acad Sci USA 70:1339–1343
Pinto da Silva P, Branton D (1970) Membrane splitting in freeze-etching. Covalently bound ferritin as a membrane marker. J Cell Biol 45:598–605
Pinto da Silva P, Kachar B (1980) Quick freezing vs. chemical fixation: Capture and identification of membrane fusion intermediates. Cell Biol Int Rep 4:625–640
Pinto da Silva P, Moss PS, Fudenberg HH (1973) Anionic sites on the membrane intercalated particles of human erythrocyte ghost membranes. Freeze-etch localization. Exp Cell Res 81:127–138
Plattner H, Bachmann L (1982) Cryofixation – A tool in biological ultrastructural research. Int Rev Cytol 79:237–304
Punter PH, Menco BPhM, Boelens H (1981) The efficacy of n-aliphatic alcohols and n-aliphatic fatty acids on various membrane systems with special reference to olfaction and taste. In: Moskowitz HR, Warren CB (eds) Odor quality and molecular structure. ACS Symposium Series 148. American Chemical Society, Washington DC, pp 93–108
Rash JE (1983) The rapid-freeze technique in neurobiology. TINS 6:208–212
Rhein LD, Cagan RH (1981) Role of cilia in olfactory recognition. In: Cagan RH, Kare MR (eds) Biochemistry of taste and olfaction. Academic Press, NY London, pp 47–68
Roof DJ, Heuser JE (1982) Surfaces of rod photoreceptor disk membranes: Integral membrane components. J Cell Biol 95:487–500
Satir BH, Satir P (1979) Partitioning of intramembranous particles during the freeze-fracture procedure. In: Rash JE, Hudson CS (eds) Freeze fracture: Methods, artifacts and interpretations, Raven Press, NY, pp 43–49
Simpson DJ (1979) Freeze-fracture studies on barley plastic membranes. III. Location of the light-harvesting chlorophyll-protein. Carlsberg Res Commun 44:305–336
Steinbrecht RA (1980) Cryofixation without cryoprotectants. Freeze substitution and freeze etching of an insect olfactory receptor. Tissue and Cell 12:73–100
Usukura J, Yamada E (1978) Observations on the cytolemma of the olfactory receptor cell in the newt. 1. Freeze replica analysis. Cell Tissue Res 188:83–98
Verkleij AJ, Ververgaert PHJTh (1975) The architecture of biological and artificial membranes as visualized by freeze-etching. Ann Rev Phys Chem 26:101–122
Wade JB (1976) Membrane structural specialization of the toad urinary bladder revealed by the freeze-fracture technique. II. The mitochondria-rich cell. J Membr Biol 29:111–126
Warner FD (1981) Structure-function relationships in cilia and flagella. In: Harris JR (ed) Electron microscopy of proteins, Vol 1. Academic Press, London NY, pp 301–344

Accepted October 16, 1983